Tectonophysics 606 (2013) 140–159

Contents lists available at ScienceDirect

Tectonophysics

journal homepage: www.elsevier.com/locate/tecto

Crustal structure across northeastern Tibet from wide-angle seismic profiling: Constraints on the Caledonian Qilian orogeny and its reactivation

Zhongjie Zhang [a,*], Zhiming Bai [a], S.L. Klemperer [b], Xiaobo Tian [a], Tao Xu [a], Yun Chen [a], Jiwen Teng [a]

[a] State Key Laboratory of Lithospheric Evolution, Institute of Geology and Geophysics, Chinese Academy of Sciences, Beijing, China
[b] Department of Geophysics, Stanford University, Stanford, CA 94305-2215, USA

ARTICLE INFO

Article history:
Received 10 September 2012
Received in revised form 18 February 2013
Accepted 27 February 2013
Available online 13 March 2013

Keywords:
Wide-angle seismic profiling
Crustal structure
Channel flow
Growth of plateau
Northeastern Tibet

ABSTRACT

The northeastern Tibetan plateau results from the superposition of the Caledonian Qilian orogenic belt and Cenozoic reactivation following continental collision between the Indian and Asian plates. In order to identify the constraints on the Qilian orogenic mechanism and the expansion of the plateau, we carried out a 430-km-long wide-angle seismic experiment between Jingtai and Hezuo. We herein present the crustal P-wave velocity structure model resulting from the interpretation of this wide-angle seismic dataset. The principal characteristics of the crustal velocity model include: (1) thinning of the crust from south to north within a range of about 48–54 km with some undulation of the Moho beneath the Northern Qilian block; (2) the thickness of the sedimentary layer and its average P-wave velocity exhibit the obvious tectonic division of the Qaidam–Kunlun–West Qinling belt, the central and Northern Qilian, and the Alax blocks; (3) the lower crustal layer has a P-wave velocity of 6.6–6.8 km/s beneath the Qaidam–Kunlun–West Qinling belt, Northern Qilian orogenic belt and Alax block, but has a very low value of 6.4–6.5 km/s beneath the Central Qilian block; and (4) the Central Qilian block shares a similar crustal P-wave velocity–depth relationship with the Sierra Nevada arc or the accretionary crust. The Qaidam–Kunlun–West Qinling and the Northern Qilian orogenic belts have a crustal P-wave velocity–depth relationship characteristic of the crust of the global average continent. The particular Vp–depth relationship beneath the Central Qilian orogenic belt may result from a Caledonian accretionary orogeny or from the delamination of the ecologized lower crust during the arc–continental collisional orogeny. The lower velocity layer (LVL) exists at the bottom of the upper crust, to the north of the middle of the central Qilian block. We infer that this LVL plays an important role as an intracrustal decollement to expand the plateau.

1. Introduction

The Tibetan plateau covers a vast area (about 2.5 million km^2), and is characterized by a high topography (with an average altitude of 4000 m above sea level) and a thick crust (with an average crustal thickness of 60–75 km). Both the process itself and the mechanism of the crustal thickening, as well as the lateral expansion of the plateau, are among the key topics in the study of the continent–continent collision involved in forming the Tibetan plateau (Yin and Harrison, 2000). This is related to the subduction, collision and postcollisional convergence of the PaleoTethys and NeoTethys plate and the associated continental lithosphere (Royden et al., 2008; Tapponnier et al., 2001). Numerous models have been proposed, such as wholesale underthrusting (Argand, 1924), the injection of the crust of India beneath that of Asia beneath South Tibet (Himalaya, Lhasa terranes) (Zhao and Morgan, 1985), channel flow or extrusion of the middle crust in Himalaya (Beamount et al., 2004; Klemperer, 2006; Zhang and Klemperer, 2010) to uplift the plateau and middle/lower crustal channel flow (Royden et al., 2008), or tectonic escape (Burchifel et al., 1989; Tapponnier et al., 2001; Zhang et al., 2010a,b) in Eastern Tibet, causing the lateral expansion of the plateau (Klemperer, 2006). All these models can be categorized into distributional shortening/thickening of the Asian crust (Dewey and Burke, 1973; Mattauer, 1986; Molnar and Lyon-Caen, 1988; Molnar and Tapponnier, 1978) and the homogeneous shortening/thickening of the Asian lithospheric mantle with convective removal of its lithospheric bottom (Dewey et al., 1988; England and Houseman, 1986, 1989; Molnar, 1993; Zhang et al., 2009, 2010a,b). It should be mentioned that most of these models have been proposed from tectonic (Yin and Harrison, 2000) or geophysical observations (Nelson et al., 1996; Owens and Zandt, 1997; Zhang and Klemperer, 2010; Zhao and Nelson, 1993) in the Himalayas and within the plateau bounded by Main Boundary Thrust (MBT) (to the south) and the Kunlun fault (to the north), with more interest being paid to the shallow characteristics and deep structure south to the Kunlun fault (i.e., at its northern edge) (Jia et al., 2009; Li et

* Corresponding author. Tel.: +86 10 82998313.
E-mail addresses: zhangzj@mail.iggcas.ac.cn (Z. Zhang), sklemp@pangea.stanford.edu (S.L. Klemperer).

0040-1951/$ – see front matter © 2013 Elsevier B.V. All rights reserved.
http://dx.doi.org/10.1016/j.tecto.2013.02.040

al., 2003; Liu et al., 2006; Tian and Zhang, in press; Wang et al., 2005; Zhang et al., 2011a,b,c,d). However, to the north of the Kunlun fault, from the Tarim, Gobi and Alax platforms (Fig. 1), the fold–thrust belts along the northeastern edge of the Tibetan plateau (such as the Henan Shan, Qilian Shan, and Liupan Shan) are presently undergoing shortening as they are incorporated into the plateau (Meyer et al., 1998).

In tectonic terms, the northeastern Tibetan plateau is a mosaic of multiple terrains and island–continental arcs (Xu et al., 2001). Lying in the northern margin of the Tibetan plateau, the Qilian Caledonian orogenic belt forms a WNW-ESE trending belt with a length of about 800 km and a width of 400 km (Xu et al., 2001). This belt is bounded to the north by the Hexi Corridor, by the Qaidam basin to the south, by the West Qinling Mountains to the east and by the Altyn Tagh fault to the west (Xu et al., 2001). The northeastern Tibetan plateau can be divided into five tectonic units; these are, from north to south, the Alax block, the North Qilian oceanic-type Suture Zone (ONQ), the Qilian block, the North Qaidam continental-type UHPM belt (CNQ) and the Qaidam Kunlun–West Qinling block (Fig. 1). The discoveries of the HP/LT metamorphic belt and the North Qaidam UHP metamorphic belt in northeastern Tibet (Song et al., 2002, 2009; Yang et al., 1998; Yin et al., 2007a,b) provide important constraints on our understanding of the Caledonian orogeny. It is now accepted that the Qilian terrane has a Caledonian arc–continent orogeny. Essentially there are three possible orogeny mechanisms, namely (1) the paired subduction model of Yang et al. (2002), (2) the transition model from oceanic subduction to continental collision of Song et al. (2006) or (3) the multiple-accretionary model of Xiao et al. (2009). There is still some uncertainty over the deep structure, the proper identification of which will allow us to determine which of the three mechanisms is responsible for explaining the convergence and collision of the Alax, the Qilian, and the Qaidam–Kunlun–West Qinling terrains, during the Caledonian.

The deep seismic sounding of the crustal structure in northeastern Tibet is important for deepening our understanding of the growth of the plateau, as well as our understanding of the Caledonian orogeny. The expansion of the plateau can be demonstrated using GPS measurements from across northeastern Tibet (Gan et al., 2007). The available mechanisms for the lateral expansion of the Tibetan plateau (to 2.5–3.0 million km^2) include (1) the northward thrusting of the upper crust (Metivier et al., 1998; Tapponnier et al., 1990); (2) tectonic escape at the crustal/lithospheric scale from lateral shearing of the Kunlun and Altyn faults (Tapponnier et al., 2001), (3) lower crustal channel flow (Royden et al., 2008) and (4) southward subduction of North China craton (Yin, 2010) from geological mapping, balanced reconstruction, tectonic, geochemical and topography data. The gradual northeastward decrease in elevation across the northeastern border of the Tibetan plateau may be taken to imply that much of the upper crust of this region forms a northeastward tapering wedge decoupled from the underlying lowermost crust and mantle lithosphere along a large lower to mid-crustal decollement dipping at a shallow angle to the southwest (Tapponnier et al., 1990, 2001). It is clear that the crustal structure across the northeastern part of the Tibetan plateau can provide constraints on our understanding of the northward growth of the plateau.

The remainder of the paper is structured as follows. In the next section, we will briefly introduce tectonics of northeastern Tibet. After that, seismic acquisition, seismic analyses and seismic interpretation are presented. After the presentation of crustal P-wave model along the profile and its evaluation, we made some discussions of the crustal velocity model on the constraints in the Caledonian Qilian orogeny and its reactivation (lateral expansion of the plateau).

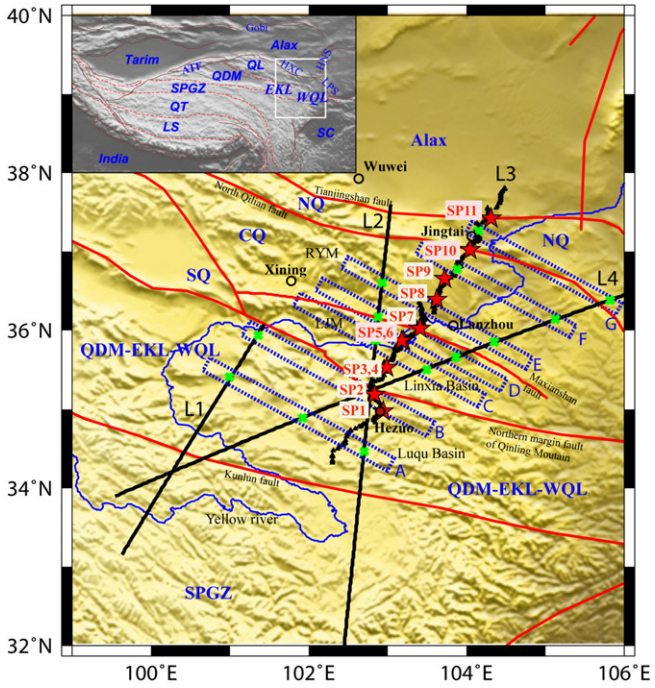

Fig. 1. Top left inset: Main tectonic units that make up the Tibetan plateau (from south to north, LS: Lhasa block; QT: Qiangtang block; SPGZ: Songpan–Ganzi block; QDM: Qaidam basin; QL: Qilian block; EKL: East Kunlun orogenic belt; WQL: West Qinling orogenic belt) and surrounding regions (India: India plate; Tarim: Tarim basin; Alax: Alax depression in the western North China craton); ATF: Altyn Tagh fault; HXC: Hexi Corridor; HNS: Henan Shan; LPS: Liupan shan. Geological map of the study area: QDM–EKL–WQL: Qaidam–East Kunlun–West Qinling block; SQ: South Qilian block; CQ: Central Qilian block; NQ: Northern Qilian block; RYM: Riyuan mountain; LJM: Laji mountain. Stars represent locations of the seismic sources (shots points SP1–SP11), and triangles represent receivers of the wide-angle seismic profile studied here. The faults crossed by the seismic profile include (from south to north): Kunlun fault, northern margin faults of Qinling Mountain, Maxianshan faults, North Qilian fault and Tianjingshan fault (Huang, 1977), the blue line denotes the course of the Yellow river. Other long seismic profiles are also drawn for comparison, namely: L1: Moba-Guide profile (Zhang et al., 2011a, 2011b, 2011c, 2011d); L2: Marking–Wuwei active source seismic transect (Jia et al., 2009; Zhang et al., 2008); L3: Jingtai–Hezuo profile (this study); L4: Darlag–Lanzhou–Jingbian seismic refraction profile (Liu et al., 2006). A. B, …, G denote different transects from south to north sampled by these four profiles, which enable us to extract different velocity–depth functions for each of these areas (delimited by dotted lines). These transects are all referenced in Figs. 6 and 9 and are mentioned in the text.

2. Brief tectonics of northeastern Tibet

Our wide-angle seismic profile extends from Jingtai to Hezuo, which crosses the Alax block, the North Qilian oceanic-type Suture Zone, the Qilian block and the Qaidam Kunlun–West Qinling block. In the following, we summarize the tectonics of these five units.

2.1. Alax block

The Alax/Hexi Corridor terrane, which is situated in the west of the Ordos Basin through the Helanshan fold belt, is at the junction of two major Chinese blocks, namely the North China and the Tarim (Fig. 1). This terrane is bounded by the Tianshan–Mongolia Fold Belt to the north and separated from Qaidam terrane by the Qilian Shan Fold Belt to the south. The western boundary of the Alax/Hexi Corridor terrane is not clearly delineated but is generally thought to lie in the vicinity of northeasterly extensions of the Altyn Tagh Fault beyond Northern Qilian Shan (Zhao and Nelson, 1993).

The Alax block in the north comprises the western part of the North China Craton, and consists predominantly of an early Precambrian basement overlain by Cambrian to middle Ordovician strata typical of the North China Craton cover sequences (Bureau of Geology and Mineral Resources of Ningxia Province, 1990).

2.2. North Qilian Suture Zone

The North Qilian Suture Zone is an elongate, NW-trending belt that lies between the Alax block (north) and the Qilian block (south) (Fig. 1). It is made up of Early Paleozoic subduction complexes including ophiolitic mélanges, high-pressure blueschists and eclogites, island–arc volcanic rocks with granite plutons, Silurian flysch formations, Devonian molasse, and Carboniferous to Triassic sedimentary cover sequences (Feng and He, 1995; Song, 1996). The ONQ is interpreted to have formed in an 'oceanic type' subduction zone in the Early Paleozoic.

The ophiolite, which is interpreted to represent the remnants of the ancient oceanic lithosphere, is well preserved in this suture zone. Geochemically, the basaltic rocks resemble present-day N- and E-type mid-ocean ridge basalt (MORB) (Feng and He, 1995; Song, 1996). Zircons obtained from a cumulate gabbro within the ophiolite suite gave U–Pb SHRIMP magmatic ages ranging from 533 to 568Ma (554 ± 16 Ma) (Yang et al., 2002). Within the suture zone there are two sub-belts of high-pressure metamorphic rocks (Song, 1996), namely (1) a low-grade blueschist belt with a typical assemblage of glaucophane, lawsonite, pumpellyite, aragonite,and albite; and (2) a high-grade blueschist belt with an assemblage of garnet, phengite, glaucophane and epidote that locally encloses massive blocks of eclogite. The protoliths of the blueschists include greywacke, marble, chert and volcanic rocks. Glaucophane and phengite Ar–Ar isotope dating have yielded ages in the range 460–440 Ma (Liou and Graham, 1989; Wu et al., 1993; Zhang et al., 2010a,b).

2.3. Central Qilian block

The Central Qilian block, located between the North Qilian Suture Zone and the Qaidam–Kunlun–West Qinling block, is an imbricate thrust belt of Precambrian basement overlain by Paleozoic sedimentary sequences. The basement consists of felsic gneiss, marble, amphibolite and localized granulite. Wan et al. (2001) reported 910–

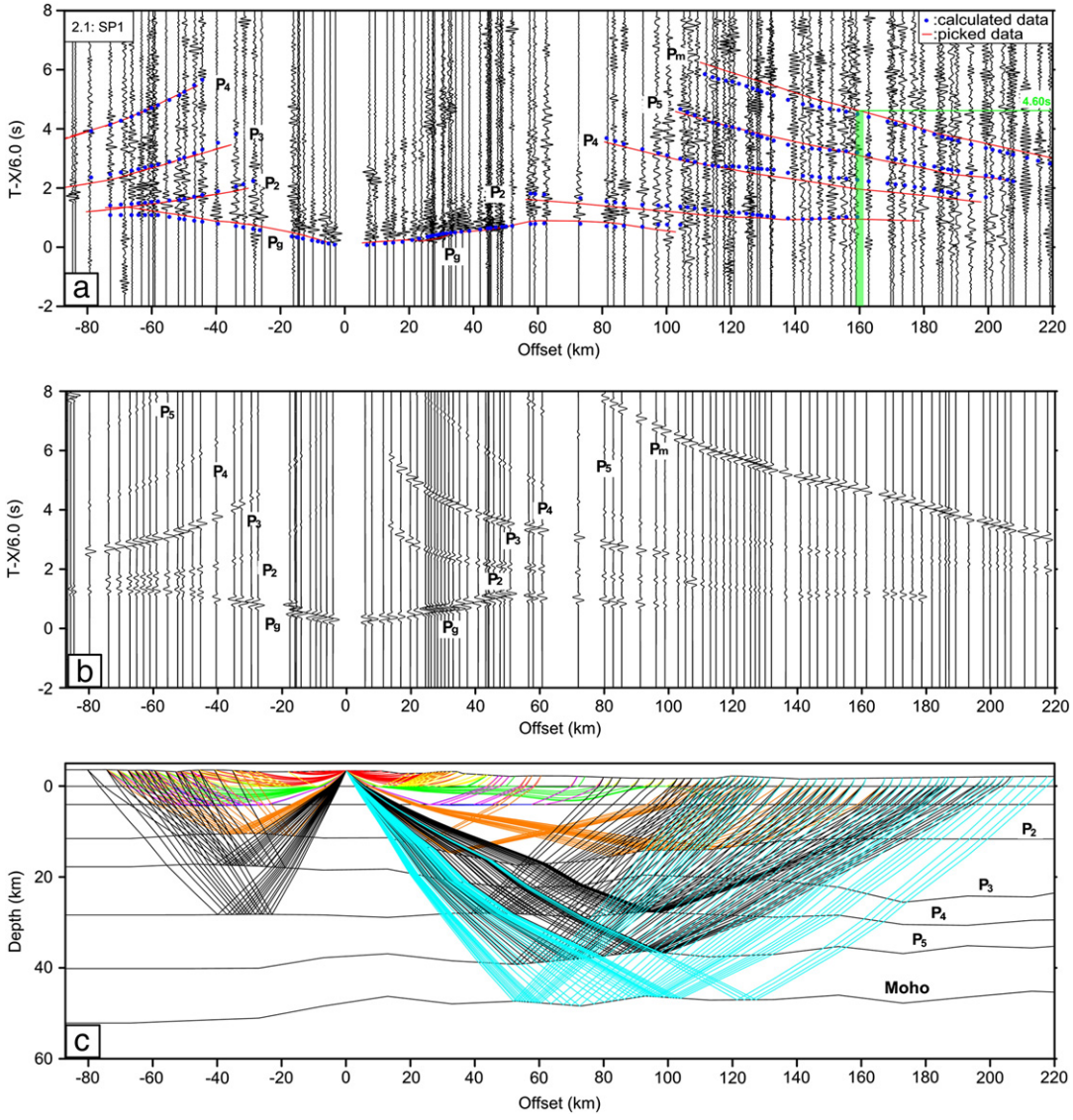

Fig. 2. Reduced P-wave seismic sections for (Fig. 2.1) shot SP1 at Hezuo, the southernmost shot of the profile; (Fig. 2.2) shot SP2 at Wangger; (Fig. 2.3) shot SP3 at Zhangzigou; (Fig. 2.4) shot SP5 at Sanyuan; (Fig. 2.5) shot SP7 at Santiaojian; (Fig. 2.6) shot SP8 at Shuping; (Fig. 2.7) shot SP9 at Qinchuan; (Fig. 2.8) shot SP10 at Jingtai; and (Fig. 2.9) shot SP11 at Wenduerlesumu, at the eastern end of the profile. Upper panels show the observed data, middle panels show the vertical component of the synthetic data, and lower panels show the corresponding ray-path of each shot point. The reduction velocity is 6.00 km/s. In the upper panels, the seismic data is filtered using a 1–10 Hz bandpass filter. The dashed lines show the seismic boundary layers calculated using the final crustal velocity model, as shown in Fig. 3.

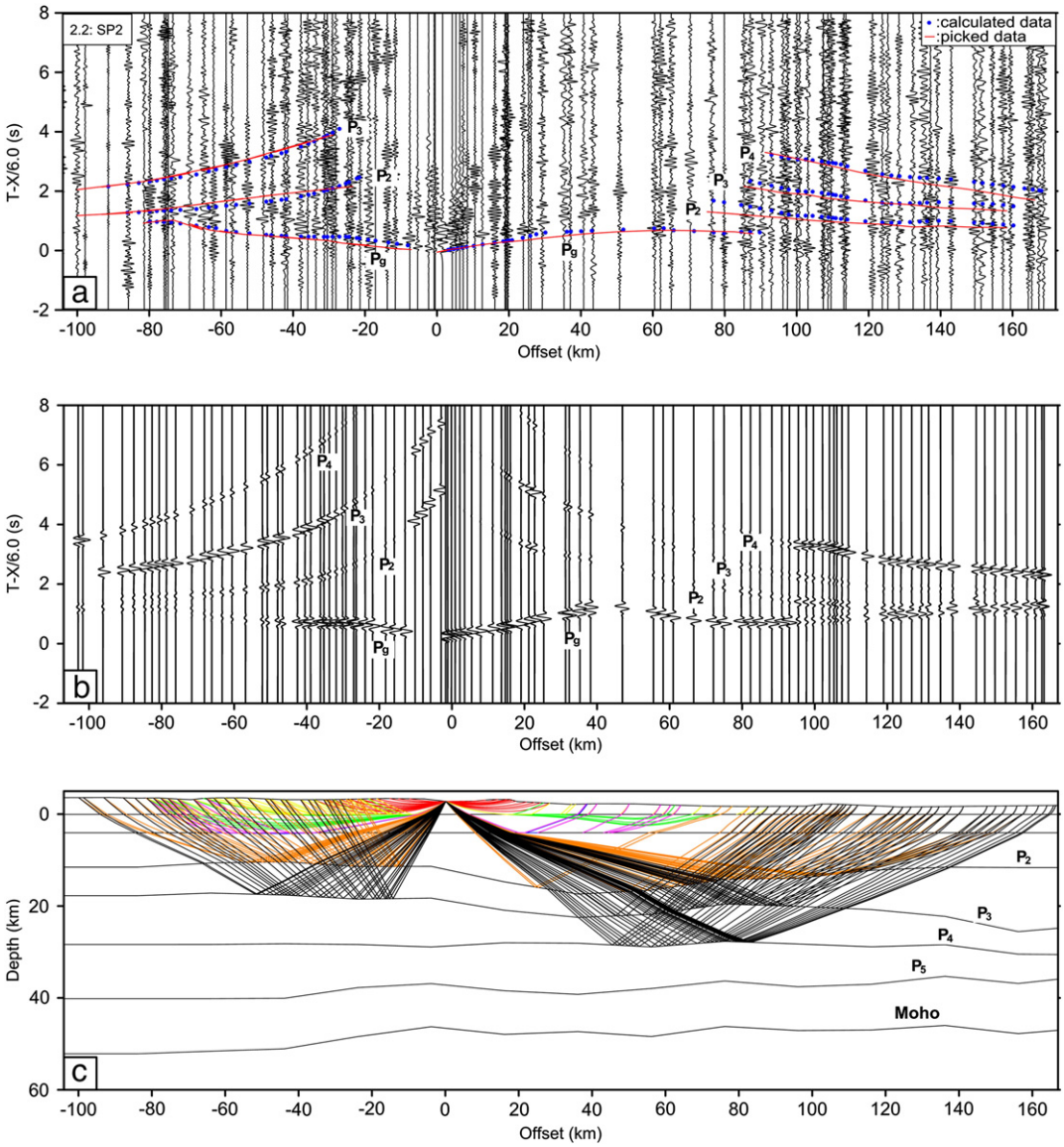

Fig. 2 (*continued*).

940 Ma single-zircon ages in granitic gneisses from different regions of the northern part of the Qilian block, which were interpreted as the ages of the formation of the protolith and are consistent with the ages of granitic gneisses from the North Qaidam UHP belt.

2.4. Qaidam–Kunlun–West Qinling block

The Qaidam block to the south is a Mesozoic intra-continental basin deposited on the Precambrian crystalline basement. Zhang et al. (2003) reported detrital zircon SHRIMP ages that mainly ranged from 1600 to 1800 Ma for a metamorphosed paragneiss obtained from the southern part of the Qaidam basin, and thus concluded that the Qaidam–Qilian Craton has an affinity with the Yangtze Craton.

The Eastern Kunlun–Qaidam Terrane is bounded by the Anyimaqen–Kunlun–Muztagh suture to the south and the southern Qilian suture to the north. In the south, surface geology mapping, tectonic studies (Xiao et al., 2009; Xu and Cui, 1996; Xu et al., 1994, 1997, 1999; Yang et al., 1998) and deep seismic sounding (Zhang et al., 2011a,b,c,d) suggest that the terrane is dominated by a broad Early Paleozoic arc, on which a younger and narrower Late Permian to Triassic arc was superposed. The northern part of the Eastern Kunlun–Qaidam terrane is mostly occupied by the Qaidam basin. Bedrock exposures are scattered along its northernmost edge, immediately to the south of the South Qilian suture.

3. Wide-angle seismic experiment and data analysis

3.1. Seismic data acquisition

The P-wave seismic data used in this study were acquired from a 430 km-long wide-angle reflection/refraction profile (Fig. 1) obtained in April and May of 2009. Two organizations were involved in acquiring the seismic data, namely the Institute of Geology and Geophysics of the Chinese Academy of Sciences, and the Geophysical Exploration Centre of the China Earthquake Administration. The holes were drilled and explosives were fired by the 6th Geophysical Abridge in the Huadong Petroleum Geology Bureau of the Sino-Petroleum Exploration Company (SINOPEC). The profile, with an azimuth near N45E, runs between Hezuo and Jingtai, which is at the southern margin of Alax block, Gansu Province (Fig. 1). A total of 11 shots were fired with an average shot spacing interval of 50 km. Two shots SP1 and SP2 (near Hezuo, Fig. 1) were fired south to the northern margin of the West Qinling Mountains (in the Qaidam–Kunlun–West Qinling block); and eight

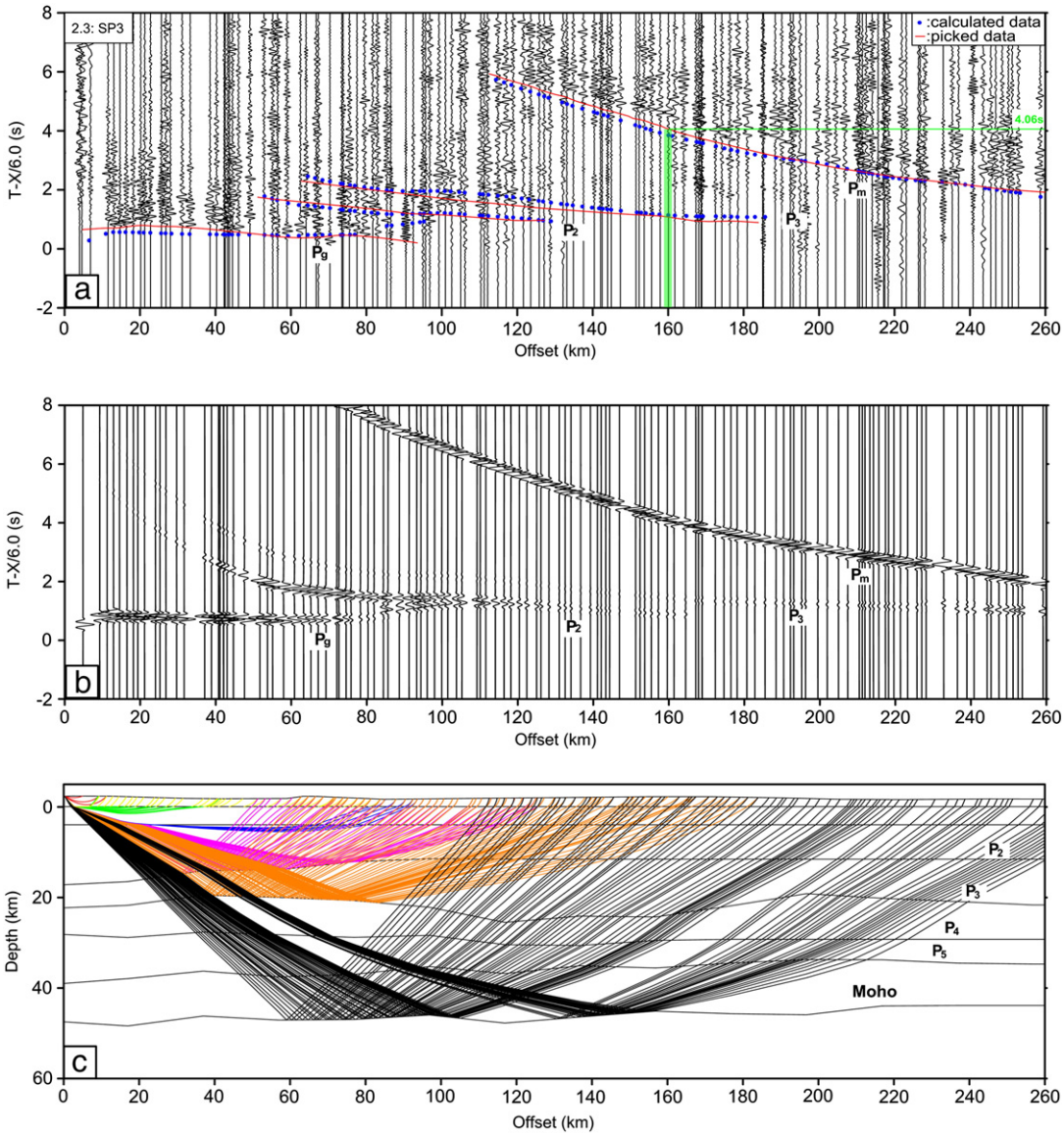

Fig. 2 (*continued*).

shots (SP3, SP4, SP5, SP6, SP7, SP8, SP9 and SP10 in Fig. 1) were fired in the Qilian terrane. SP11 is located at the northern margin fault of the Qilian Mountains and the Tianjingshan fault belt. Each shot consisted of 4–8 holes drilled to a depth of about 20–35 m and loaded with a charge containing between 1200 and 2500 kg of explosive. A total of 200 portable three-component digital seismographers were used to acquire the seismic data along the long-offset profile. The station spacing was 2 km. The 3-minute-long seismic signals provided by digital instrumentation in the course of the experiment were initially sampled at a rate of 200 sps, and then band-pass filtered within the 1–10 Hz frequency band for P-waves. In order to save space, Fig. 2 shows the P wave seismic shot gathers, reduced by a velocity of 6.0 km/s.

3.2. Recognition of seismic events

In this wide-angle seismic experiment, the refractions above the crystalline basement of the crust (Pg-phase) and the reflections from the Moho discontinuity (PmP- or simply Pm-phase) can easily be correlated, and so in the following we mainly focus our attention on the descriptions of the Pg and Pm arrivals.

The remarkable feature of these 11 shot gathers is the very weak reflections between the Pg and Pm phases, which may suggest that the part of the crust between the crystalline basement and the Moho interface in the northeastern Tibetan plateau is a transparent layer with weak reflection within the layer or a strong ductile layer with a high attenuation ability to absorb seismic energy.

The first Pg arrivals can be generally observed at offsets of up to 90 km, although this distance is clearly greater than 120 km in the case of the northern branch of the SP5 shot (Fig. 2.4a). From the SP5 shot, Pg arrivals with weak energy can be correlated with an offset of 90 km to the north, and with strong energy up to 130 km to the south. The Pg travel times are delayed after an offset of 60–70 km in the southern branch of the shot, but they vary abruptly in the north branch wherein the time-offset curve is a horizontal straight line. These characteristics demonstrate that the apparent P-wave velocity is nearly 6.0 km/s to the north, but much lower than 6.0 km/s to the south of the SP5 shot, where it is actually near to 4.2 km/s or even less.

The Pm-phase reflected from the Moho is clear in most shot gathers and can generally be correlated at offsets larger than 100 km (Fig. 2). The SP3 shot gather shows a distinctive change of Moho reflections at an offset of about 210 km, which suggests that the Moho topography or crustal velocity changes remarkably here, and the Moho deepens or crustal velocity decreases suddenly

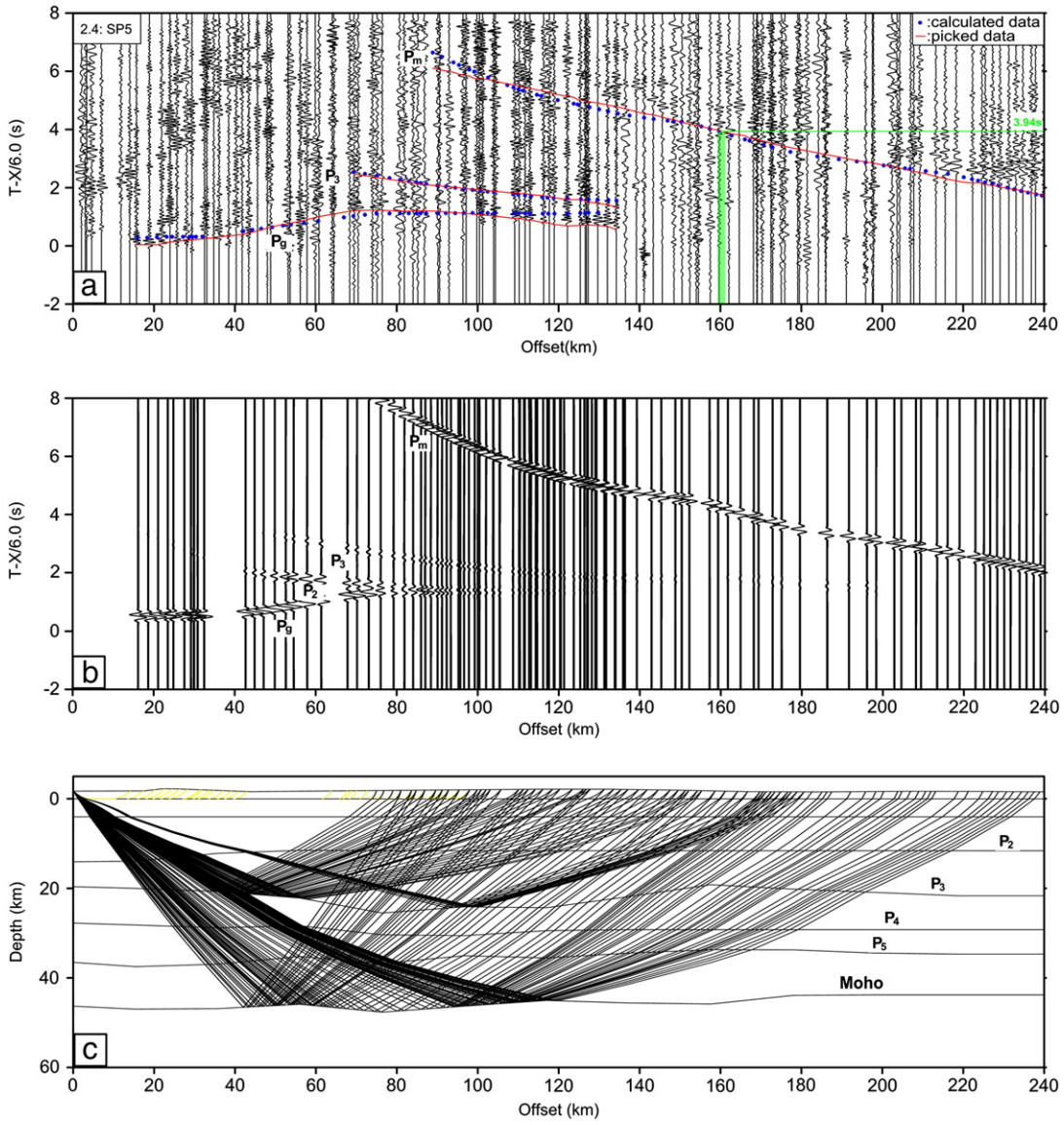

Fig. 2 (*continued*).

northeastwards. From a rough estimate of the reflection position, we found that this abrupt change in the Moho corresponds to a Pg travel time delay in the SP5 shot gather, which may suggest that there is a crustal-scale structure or fault, very likely the Maxianshan fault in the Central Qilian block.

In addition to the Pg and Pm phases, some other intra-crustal events may be seen, such as P2, P3, P4 and P5. However, not all these intra-crustal phases can be observed in the same shot gathers. For example, on the most southwesterly shot gather (Fig. 2.1), P2 and P3 are both apparent, but no P4 or P5 event can be clearly recognized. For the purposes of seismic data interpretation, we modeled all these interfaces continuously along the profile. These typical seismic responses (disappearance of some intracrustal events on some gathers) are interpreted as strong lateral heterogeneity in the crust along the profile, which should result from a Caledonian orogeny with superposition of Mesozoic–Cenozoic deformation from the consecutive convergence between the Indian and Eurasian plates. Usually, the P2 phase can be traced with an offset range of 60–130 km in shot gathers, the P3 phase can be observed with an offset range of 60–190 km, the P4 phase can be observed with an offset range of 60–140 km, and the P5 with an offset range of 80–160 km (Fig. 2.1–9).

Although the reduced travel time curves show the influence of the shallow thick sedimentary layers, they hardly show any lateral velocity variations in the crust. Reflection events from a crustal interface (labeled P2 in Fig. 2) delineate the upper crust. Other reflection events from deeper interfaces above the crust–mantle discontinuity (labeled P3 and P4 in Fig. 2) delineate the middle/lower crust.

The subcrustal Pn-phase refracted from the topmost upper mantle cannot be recognized in all 11 shot gathers of this experiment, which may be common in the Tibetan plateau because there was no recognition of the Pn phase in any of the previous wide-angle seismic experiments, including those in Himalaya (Gao, 1990; Hirn, 1988; Makovsky et al., 1999; Teng, 1987; Xiong and Liu, 1997; Zhang and Klemperer, 2010), Lhasa (Hirn et al., 1987; Makovsky et al., 1999; Min and Wu, 1987; Zhang and Klemperer, 2005; Zhao et al., 2001); Qiangtang (Jiang et al., 2006; Zhao et al., 2001); Songpan–Ganzi and Kunlun (Jiang et al., 2006; Zhang et al., 2008, 2011a,b,c,d). Therefore, in the following modeling interpretation of this seismic dataset, we choose a P wave velocity of 8.0 km/s for the topmost part of the mantle in reference to the Pn travel time tomography results (Liang and Song, 2006). The absence of any recognition of a Pn event may suggest a complicated Moho structure with strong interaction between the crust and the mantle, which is

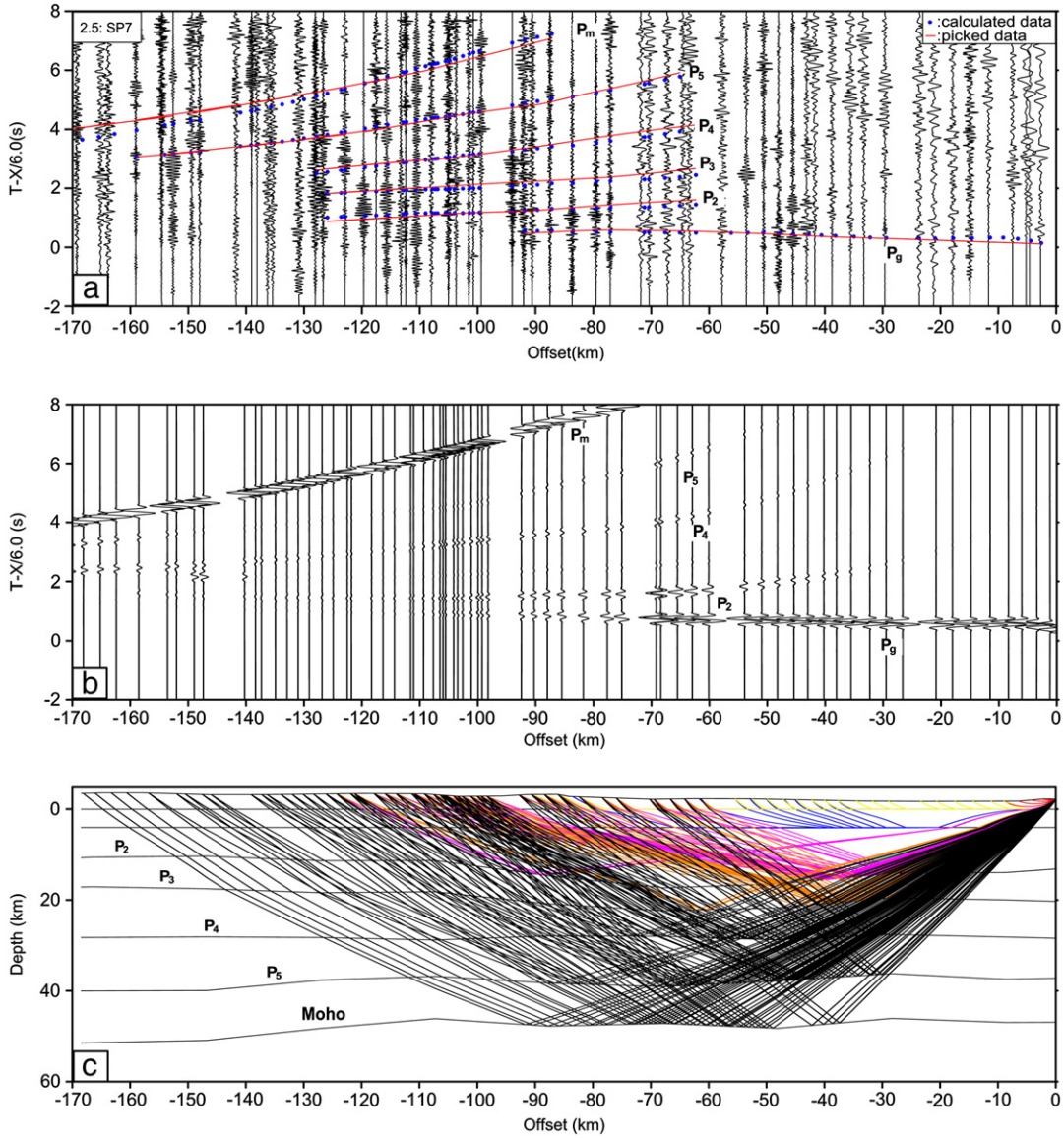

Fig. 2 (*continued*).

considered using a 1st order strong crust/mantle discontinuity in the data interpretation.

4. Data inversion and reliability tests

4.1. inversion and implementation

In order to model the seismic events described above, we began by constructing 1-D velocity–depth models using the travel times for each shot using a homogeneous and horizontal layering model. These 1-D models were then combined to provide a starting model for calculating a 2-D velocity model. The 2-D model was constructed using a combination of trial-and-error forward modeling of travel times and amplitudes (Cerveny et al., 1984), and inverse modeling of travel times for the shallow structure (Ammon and Vidale, 1993). For the travel time modeling, the forward problem was solved using classical ray-tracing techniques for the reflected phases (Cerveny et al., 1984), and an eikonal equation finite-difference solver for the first arrival of the refracted phases (Ammon and Vidale, 1993; Vidale, 1988). The partial derivatives of the calculated travel times with respect to the velocity and interface nodes were then derived. A damped least-squares inversion was then applied (Hole and Zelt, 1996) in order to obtain updates for the velocity and interface nodes, and the forward and inverse problems were then repeated until an acceptable convergence between the observed and calculated travel times was obtained, thus yielding the final velocity model of Fig. 3.

The travel time modeling was carried out using a top-to-bottom approach from the upper to the middle and lower crust. In all, 735 Pg, 278 P2P, 566 P3P, 386 P4P, 305 P5P and 639 PmP readings of travel time were used in the inversion. After eight or nine iterations, the residual travel time for each phase was 0.126s for Pg, 0.156s for P2P, 0.162s for P3P, 0.164s for P4P, 0.167s for P5P and 0.192s for PmP (Fig. 4a). In order to supplement and guide the travel time modeling, the amplitudes were calculated using dynamic ray tracing (Cerveny et al., 1984). Synthetical seismograms (the central panels in Fig. 2.1–9) can reproduce the seismic events of Pg and Pmp events and other intracrustal reflections. The predicted strong PmP reflection amplitudes could barely be observed in our recordings, which could imply a high attenuation of seismic waves in the lower crust throughout the profile.

The P-wave velocity model between Luqu and Alax basin was obtained by finite-difference calculation of travel times (Ammon and Vidale, 1993; Vidale, 1988) and depth-to-layer interface inversion from reflected phases (Hole and Zelt, 1996). The first step in

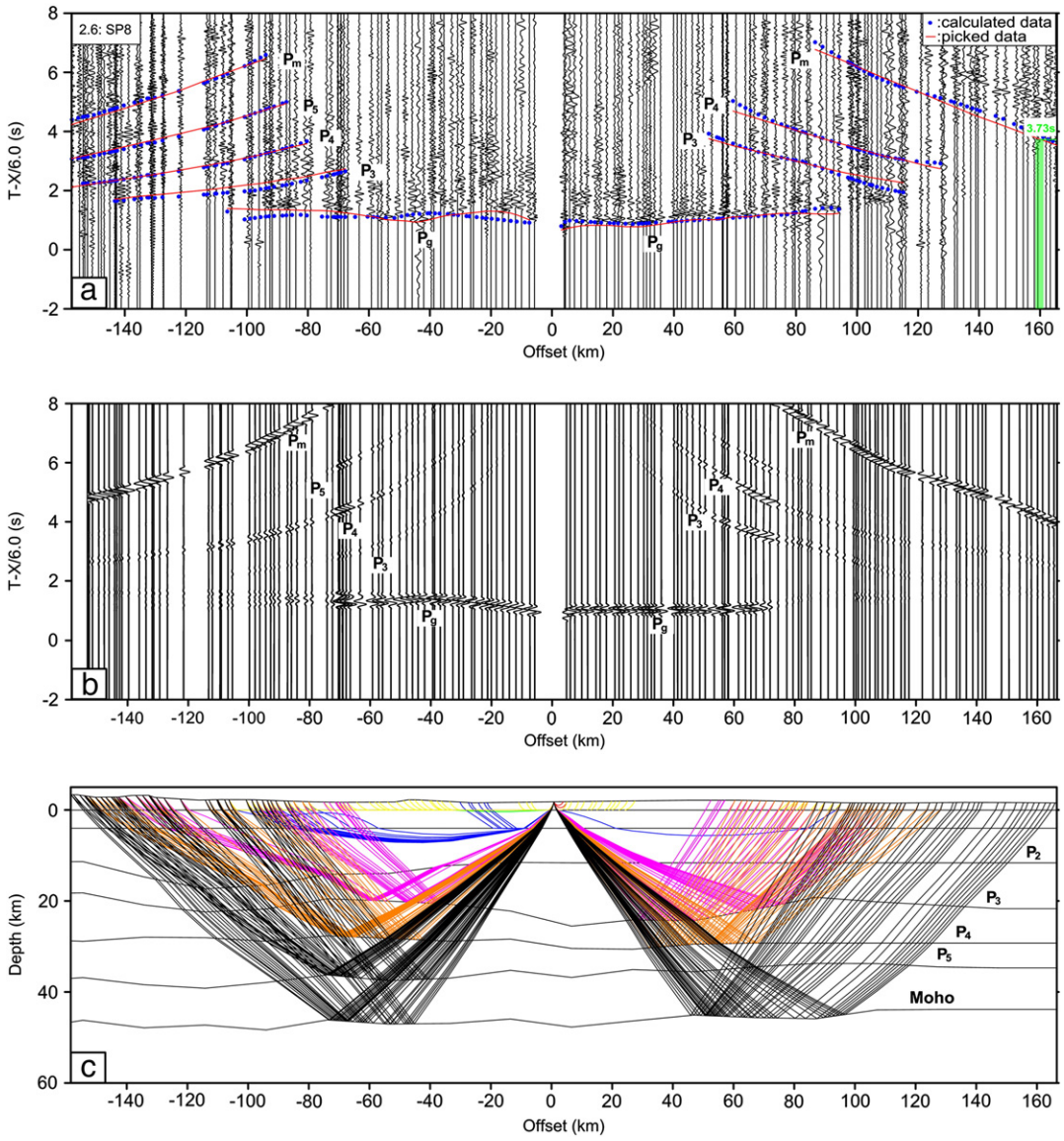

Fig. 2 (*continued*).

the procedure is (a) the modeling of the upper crust (~0–15 km depth) from velocities only, using an inversion method to predict travel times and ray paths from the selected Pg data. The second step is (b) the determination of the middle- and lower-crust velocities by inversion of PmP travel times. The third step consists in (c) depth-to-layer interface inversion from the Pm-phase and intra-crustal reflections P2, P3 and P4 (Hole and Zelt, 1996) in combination with interactive forward ray-tracing (Luetgert, 1988), but preserving the middle- and lower-crust velocities. After constraining the upper- and middle-crust velocities we interactively derive the depth and morphology of the Moho and simultaneously refine the lower-crust velocities from the Pm-phase. Therefore, the implementation of the procedure needs both an interactive ray-tracing method (Luetgert, 1988) and a finite-difference depth-to-layer interface-inversion scheme (Hole and Zelt, 1996) to model the P2, P3, P4, and Pm arrivals and the Moho depth.

4.2. Assessment of the uncertainty of the interpretation of the crustal velocity model

Seismic velocity determinations generally yield lower errors than depth determinations. Generally, seismic velocities are accurate to within 3% or ±0.2 km/s, and boundary depths, including the Moho, are accurate to within 10% of the stated depth (e.g. Mooney and Braile, 1989).

The reliability of the final velocity model initially depends on the shot point spacing, number of installed receivers, density of seismic rays, and type and quality of identified arrivals. We assume that the model is well constrained by all these factors. Nevertheless, the illumination of the crust by ray coverage along the wide-angle seismic profile is shown in the lower parts of Fig. 2. Most of the crust, particularly its wide middle part, is sufficiently tested and therefore illuminated by seismic rays, except for the zones at the extreme north and south ends of the profile. The portions either not covered by seismic rays, or those insensitive to changes in the crustal parameters, are not taken into account in the interpretation. Fig. 4b shows the ray coverage of the whole crust by the reflection phases, indicating that the majority of the crust is illuminated rather well by this wide-angle seismic experiment.

The validity of our final crustal velocity model was demonstrated by the satisfactory match between the travel times of the predicted P waves (the dashed lines in Figs. 2 and 4a) and the visible phases. It is worth mentioning that the predicted strong PmP reflection amplitudes are barely observed in the recordings (lower panels of Fig. 2), which could imply a high attenuation of the viscous lower crust (due to partial

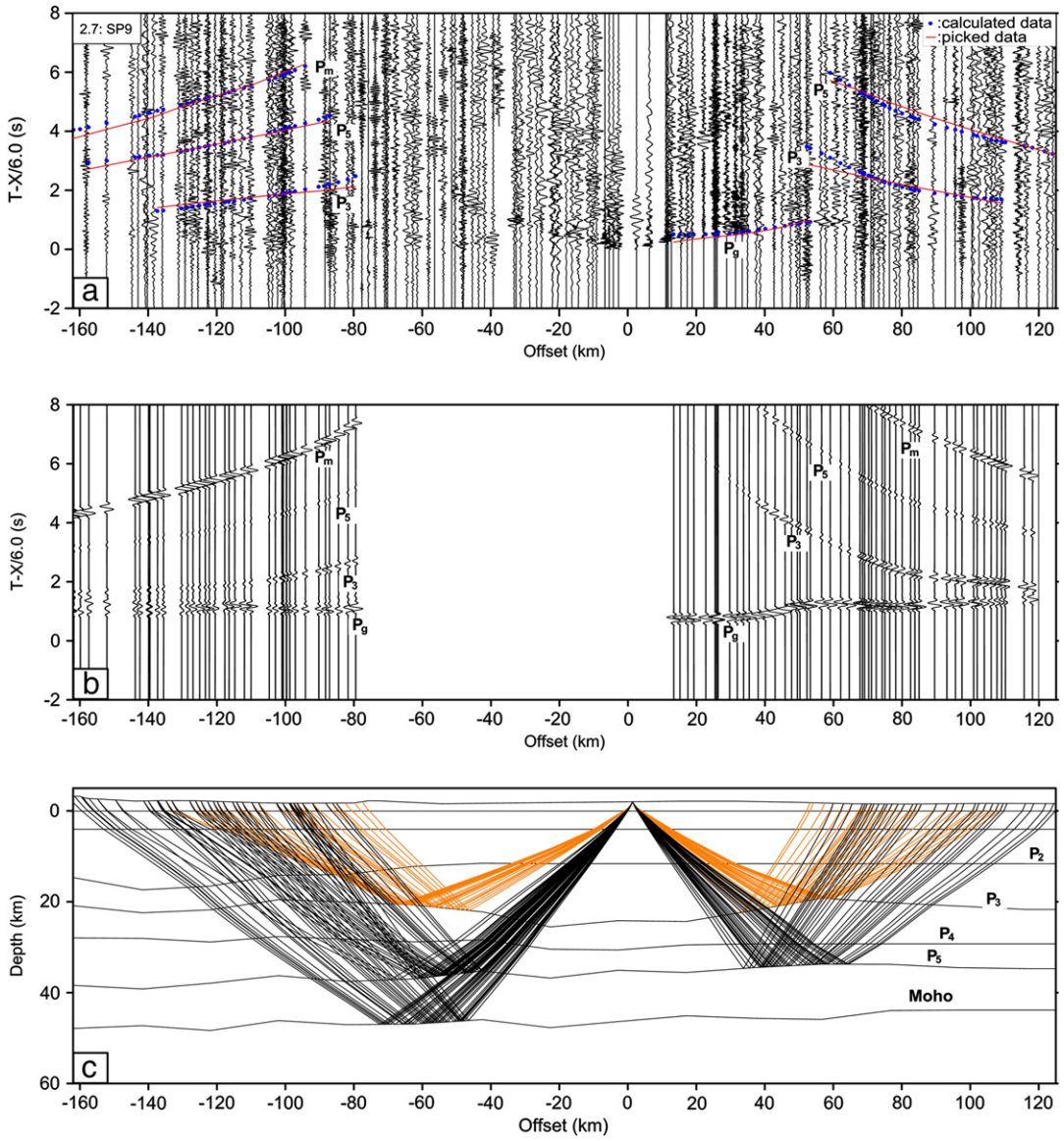

Fig. 2 (*continued*).

melting, fluids) throughout the profile, or short wavelength heterogeneities, anisotropy and vertical or subvertical structures, leading the Moho discontinuity to act not as a strong seismic wave velocity gradient belt, but as a weak one.

Another way of assessing the validity of a final crustal velocity model consists of performing a checker-board test to estimate the spatial resolution of the model, the procedure of which was described by Zhang et al. (2011d). Fig. 3 shows our final interpretation of the whole crustal P-wave velocity model. In order to get a sense of the lateral resolution of the preferred model, we firstly added alternating velocity perturbations of ±0.3 km/s to each velocity node and depth perturbations of ±1.0 km to each depth node of our initial crustal velocity model in the real data travel time inversion of the wide-angle seismic profile (Fig. 5a). We then computed synthetic travel time data from the perturbed model, and inverted these synthetic data to obtain a velocity perturbation pattern (Fig. 5b). We successfully recovered the checker-board pattern throughout the illuminated area of the crust, although the amplitudes of the perturbation were typically somewhat reduced. We infer a lateral resolution of about 10 km within the central part of the profile.

In order to make a further evaluation of our final crustal velocity model, we estimated the sensitivity of the objective function to a change of velocity at each node of the crust. In principle, the more sensitive (or greater) the objective function to the velocity perturbation at one specific node, the more reliable the velocity prediction at that node. Fig. 5c shows the variation of the objective function (Zhang et al., 2011c) in the travel time inversion to a variation in P-wave velocity of 0.3 km/s at each node in our final crustal velocity model. As expected, the shallow structure is better resolved than the deep structure, though acceptable velocities are seen throughout the crust (Fig. 5c).

5. Crustal velocity model along the Jingtai–Hezuo profile

The crust beneath the Jingtai–Hezuo profile can be divided into several layers, including a sedimentary layer and a consolidated crust. The consolidated crust can be subdivided into an upper and lower crust. The shallow velocity structure reveals the geometry of the sedimentary basins or depressions along our profile. Strong lateral variations in sedimentary thickness and composition may be

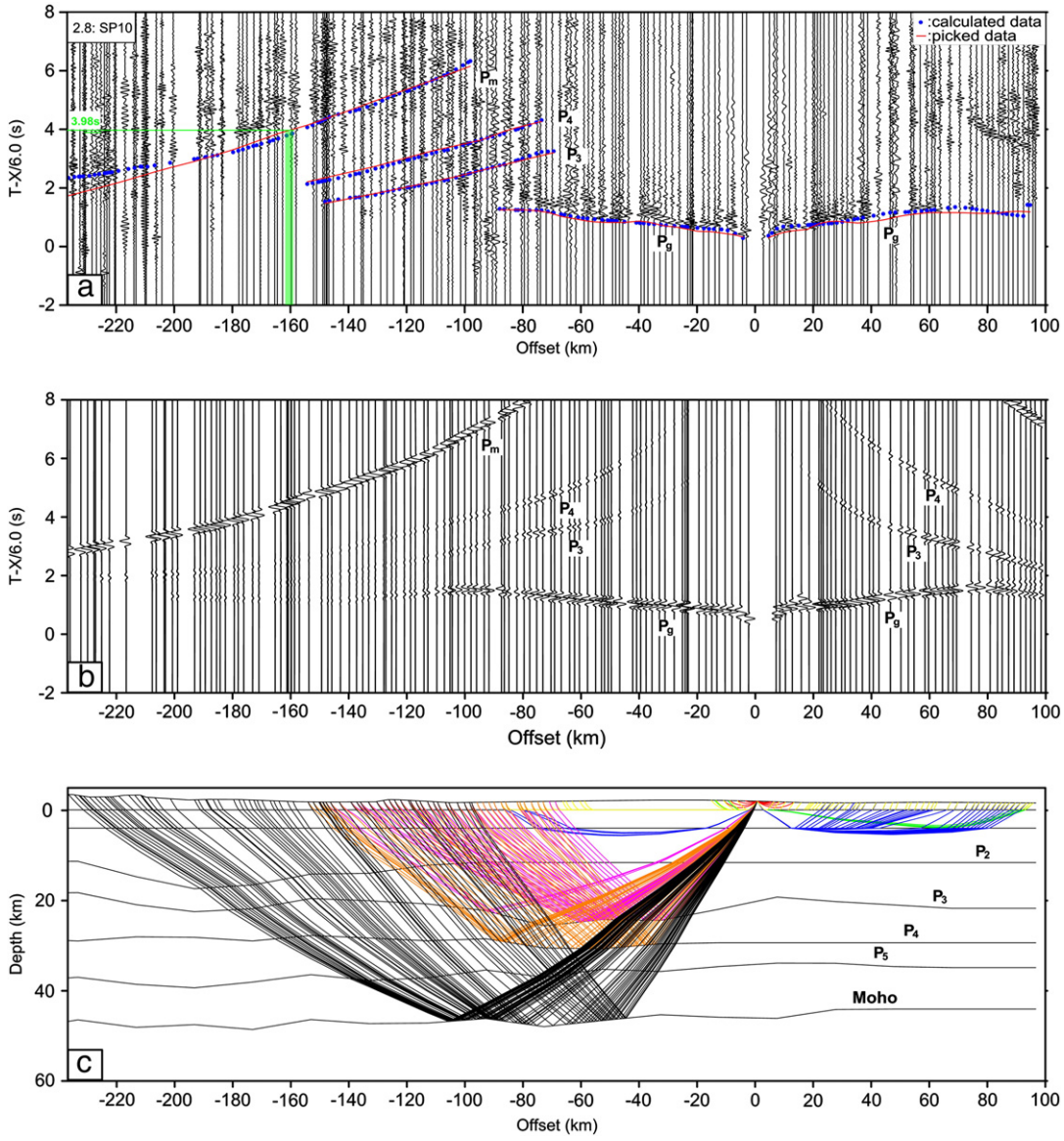

Fig. 2 (*continued*).

inferred from the variations in P-wave velocity in the range 3.8–5.9 km/s. We infer that the velocities of <4.5 km/s (which are about 1 km thick at most in our profile) represent the Cenozoic fill of the intra-montane Linxia basin (e.g. Fang et al., 2005) at the extreme north end of the profile, and the scattered Neogene/Quaternary deposits elsewhere. The velocities of <6.2 km/s are taken to represent the bottom of the upper part of the consolidated crust, and the remaining deeper section is the lower part of the consolidated crust. In the following, we discuss the crustal velocity model beneath several tectonic units along the profile: Qaidam–Eastern Kunlun–West Qinling terrane, Central Qilian Orogenic belt, Northern Qilian HP metamorphic belt and Alax block.

5.1. Qaidam–Eastern Kunlun–West Qinling domain (QDM–EKL–WQL)

The segment from the south end to about 120 km along the profile belongs tectonically to the Qaidam–Eastern Kunlun–West Qinling terrane. From our crustal velocity model, we observe that the sedimentary layer can be divided into southern and northern parts. For the southern part, the sediment thickness is about 2–4 km with a P-wave velocity <5.8 km/s. This is consistent with the widespread deposition of Middle–Upper Carboniferous shallow marine carbonate rocks, which have no volcanic clasts interrupting the Early Paleozoic volcanic activity and associated magmatism in the central and northern parts of the East Kunlun–Qaidam block. The northern part of the Eastern Kunlun–Qaidam terrane is mostly occupied by the Qaidam basin. Bedrock exposures are scattered along its northernmost edge, immediately to the south of the South Qilian suture. In this region, Ordovician shallow marine strata are interbedded with andesites and volcanic tuffs, possibly representing a back arc setting behind the south-facing Ordovician Kunlun arc, along the southern edge of the Eastern Kunlun–Qaidam terrane. The Kunlun continental arc is represented by its crustal P-wave velocity–depth relationship from the Guide-Moba profile (Zhang et al., 2011a,b,c,d).

5.2. Central Qilian orogenic belt (CQ)

The segment from 120 to 300 km on the profile (Fig. 4) belongs to the Central Qilian orogenic belt (CQ). With the boundary of Maxianshan fault, we observe the differences in structure between south and north. Beneath the southern part, the sedimentary layer thickness is just 1 km with P-wave velocity <5.0 km/s, underlain by a high velocity anomaly of Vp = 6.0–6.2 km/s, which corresponds

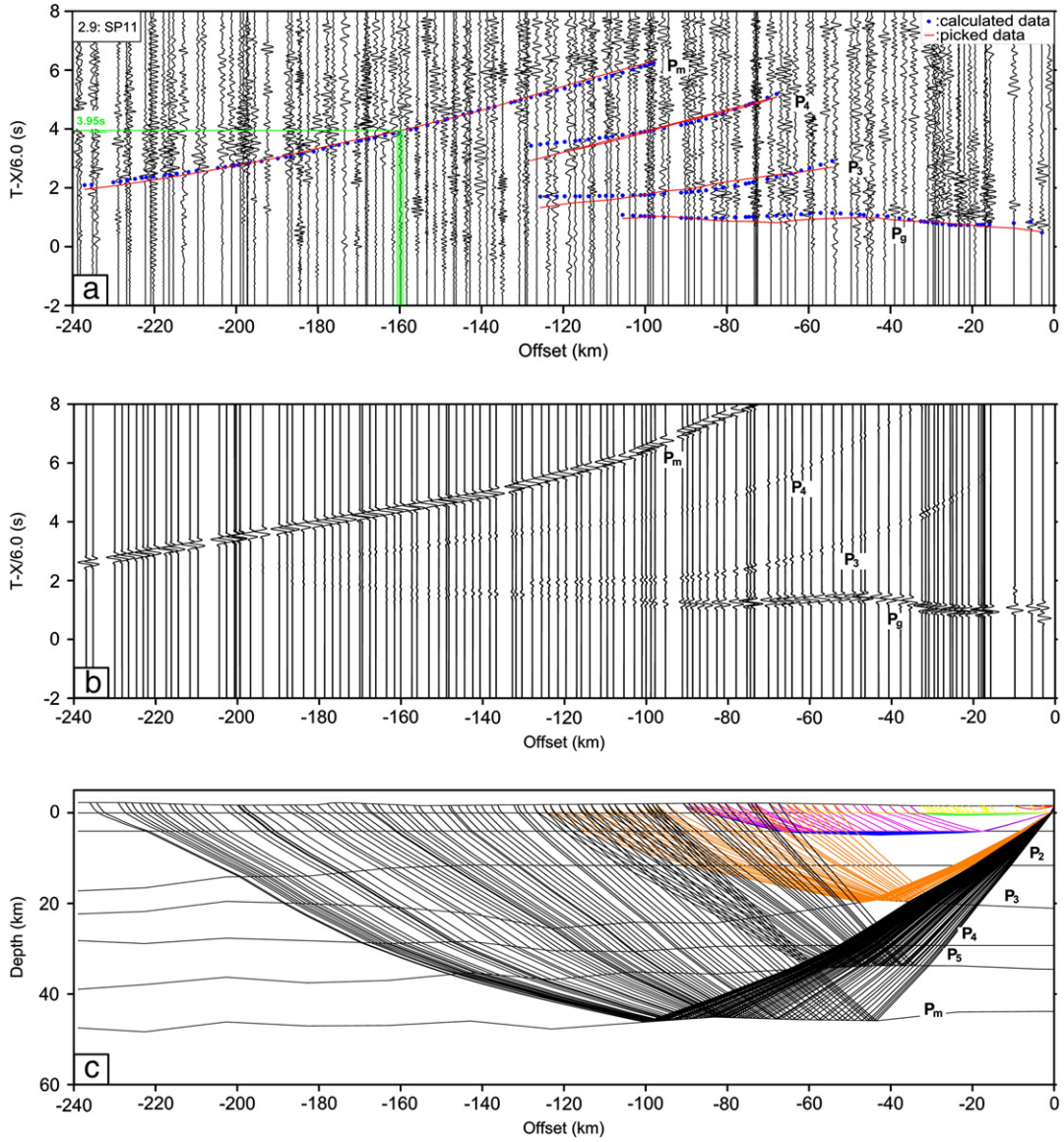

Fig. 2 (*continued*).

with the Linxia basin, located 100 km southwest of the city of Lanzhou. The Linxia basin is at the northeastern edge of the Tibetan plateau and on the western margin of the Loess Plateau. To the north lie the deserts of west/central China and Inner Mongolia (Fig. 1). The basin is 200 km long and 75 km wide at a current elevation of 2–2.6 km. The oldest documented sedimentary rocks in the basin are about 29 Ma old and the sedimentary package is more than 1 km thick. The basin fill thins and pinches out at the Maxianshan to the northeast (Fang, 1995; Fang et al., 2003). Southwest of the Linxia basin, the northeastern margin of the Tibetan plateau is delineated by the West Qinling Mountains, which are made up of Devonian through Permian metasedimentary terrestrial and marine deposits and plutons of Early Paleozoic and Late Paleozoic–Early Mesozoic age (Garzione et al., 2005 and references therein). On the northern edge of the Linxia basin, the Maxianshan is underlain by Jurassic to Paleocene terrestrial deposits (Gansu Geologic Bureau, 1989). The basin is elongate parallel to the fold thrust belt on the northeastern edge of the Tibetan plateau. Subsidence history and stratigraphic studies of three measured sections show that the Linxia basin was formed under flexural loading during the thickening of the northeastern margin of the Tibetan plateau between about 29 and 6 Ma. Between about 8 and 6 Ma the basin was incorporated into the deformation front of the Tibetan plateau (Fang et al., 2003).

Beneath the Central Qilian orogenic block, the P-wave velocity ranges from low to 6.1–6.2 km/s in the upper crust, and is less than 6.5 km/s in the lower crust (Fig. 3). The average crustal P-wave velocity between the 5.8 km/s isoline and Moho is about 6.08–6.27 km/s, much lower than the global average for the continent of 6.45 km/s (Christensen and Mooney, 1995); the average for mainland China is 6.3 km/s (Li and Mooney, 1998; Teng et al., in press; Zhang et al., 2011a,b,c,d). These probably reflect the special composition of the crust.

5.3. Northern Qilian orogenic belt (NQ)

The segment at 300–350 km on the profile (Fig. 3) belongs to the Northern Qilian block (NQ). It is a NW-SE trending Caledonian orogenic belt as part of an elongate, NW-trending belt that lies between the Alax block to the north and the Qilian block to the south.

In our crustal P-wave velocity model we observe that there are 3–4 km thick sediments underlying the crystalline basement with a P-wave velocity of 5.8–6.0 km/s. The continuity of the 2–3-km layer

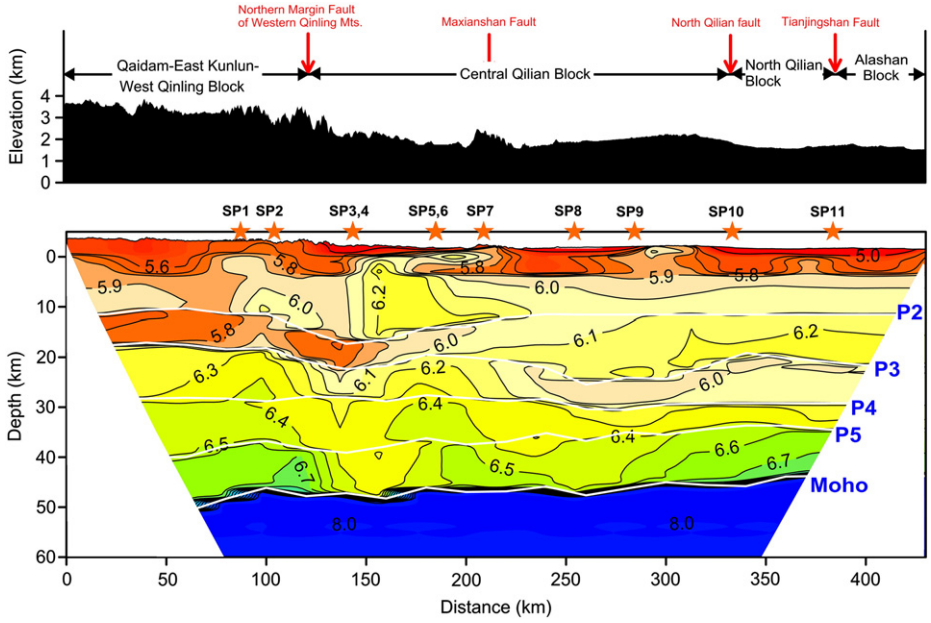

Fig. 3. Crustal velocity model along the Jingtai–Hezuo profile. A description of the tectonic setting is given above the profile. The lines shown in color are constrained by rays.

with P-wave velocities of 5.8 and 5.9 km/s beneath the Alax, the Northern Qilian block, and even most part of the Central Qilian orogenic block (Fig. 3), may provide support for the theory that the Qilian block lies at the western margin of North China craton (Yin et al., 2002). With the boundary at 375 km, the sedimentary layer of the Northern Qilian HP metamorphic belt can be divided into southern and the northern sub-belts. The sediments are a little thicker beneath the southern than the northern sub-belt, which may correspond to a southern high-grade blueschist belt and a northern low grade blueschist belt, as seen from surface geology mapping (Song et al., 2006; Meng and Zhang, 2000; Zhang et al., 2010a,b).

Beneath the Northern Qilian block, we observe that the P-wave velocity increases from about 6.2 km/s at about 15–20 km deep, to 6.6–6.7 km/s in the lower crust. There is an approximately 5-km-thick lower velocity layer (Vp–6.0 km/s) interbedded in this layer, with a P-wave velocity of 6.1–6.2 km/s. The average crustal P-wave velocity between the 5.8 km/s isoline and Moho is about 6.0–6.1 km/s, much lower than the global average for the continent of 6.45 km/s (Christensen and Mooney, 1995); the average for mainland China is 6.3 km/s (Li and Mooney, 1998; Teng et al., in press; Zhang et al., 2012a,b).

5.4. Alax block

Given the limitations of the seismic observation system, the lower crustal structure beneath the Alax block is unresolved because it lacks PmP refection data. Here, we introduce data only for the upper crust, imaged using a seismic dataset obtained from this wide-angle seismic experiment. We observe that above the 2–3-km-thick layer with a P-wave velocity of 5.8–5.9 km/s, there are 3–4 km-thick sediments beneath the Alax depression with a P-wave velocity of about 5.0 km/s (Fig. 3). This observation should reflect the predominance of an early Precambrian basement overlain by Cambrian to middle Ordovician strata typical of the North China Craton cover sequences.

6. Discussion

6.1. Comparison with previous studies

The structures of the crust and upper mantle in different segments of the northeastern Tibetan plateau have, since the 1980s, been studied by means of a range of controlled source seismic experiments (Zhang et al., 2011a,b). The active source seismic profiles have included the Moba-Guide wide-angle seismic profile (Zhang et al., 2011c; L1 in Fig. 1), the Markang–Wuwei seismic profile (Jia et al., 2009; Zhang et al., 2008; L2 in Fig. 1); our Jingtai–Hezuo profile (this study; L3 in Fig. 1) and the 1000 km-long Darlag–Lanzhou–Jingbian seismic refraction profile (Liu et al., 2006; L4 in Fig. 1).

We choose several 1D crustal columns in the corresponding profiles to discuss the west–east variation of the crustal structures in different tectonic units (Fig. 6), and then make the corresponding comparisons of the Vp–depth curves. All four profiles pass through the QDM–EKL–WQL terrane (Fig. 6), and all profiles except L1 pass through other tectonic blocks along the profiles, such as the Central Qilian block, the north Qilian block, and the Alax block (Fig. 1).

Panels A and B in Fig. 6 show our comparisons of Vp–depth between west and east (among profiles L1, L2, L3 and L4 in panels A and B) and also between south and north (panels A and B) in the Qaidam–Kunlun–West Qinling terrane. From panel A in Fig. 7, we observe that the Moho depth is about 52 km beneath profile L4, consistent with the L3 profile, but 5–8 km shallower than beneath the L1 and L4 profiles. This difference in Moho depth (or crustal thickness) should be attributed to the west–east variations in crustal thickness. By taking the P2 reflector as the boundary between the upper and the lower crust, we observe that the lower crust is about 5–8 km thicker beneath the west (L1, L4 profile) than beneath the east (L2, and L3 profile). By comparing panels A and B in Fig. 6, we observe that this west–east variation decreases from the south to the north.

Profiles L2, L3 and L4 pass through the Central Qilian block, and we choose four columns C, D, E and F in this terrane (the positions of C, D, E, F can be seen in Fig. 1) to discuss the west–east and south–north variation in crustal structure by comparing their Vp–depth curves. From panels C, D, E, and F in Fig. 6, we can evaluate (1) the west–east variation in the crust through the comparisons of Vp–depth among profiles L1, L2 and L3 in each column and (2) the north–south variation in the crust beneath the Central Qilian terrane by comparing the four panels. The Vp–depth curves in the four panels of Fig. 6 show that there is an important boundary of the Maxianshan fault as a crustal scale fault that separates the southern and northern parts of the Central Qilian block in terms of different trends in the west–east variation of crustal thickness. South of the fault, we

observe that lower crust thickening is more obvious beneath the east than the west (beneath columns C, D); north of the fault (columns E and F) lower crustal thickening increases from west to east. While we do not understand the significance of this fault, we speculate that the fault may be related to the transition of the oceanic crust (southward) subduction, and to the delamination of the ecologitized lower crust beneath the south of the fault (with no intermediate or mafic composition of the lower crust) (Fliedner et al., 2000).

There are two active source seismic profiles (L3 and L4) passing through the Northern Qilian block (Fig. 1), and we make comparisons of the 1D crustal structure between these profiles in column F (Fig. 6). Panel F in Fig. 6 shows comparisons of the Vp–depth among profiles L3 and L4 in the North Qilian terrane, which suggests that lower crustal thickening is more obvious beneath the west (L3) than the east (L4) of the terrane.

The differences in lower crustal thickening or thinning in both the south–north and the west–east directions may reflect the difference in crustal deformation to accommodate the convergence and shortening between the North China craton and the Kunlun block.

6.2. Crustal properties of tectonic units sampled by the profile

The seismic velocities reveal differences in crustal structure and composition between the Qaidam–East Kunlun–West Qinling block, the Central and the North Qilian blocks (Figs. 3 and 6). Usually, the P-wave velocity at the crystalline basement varies between different tectonic blocks. Considering this uncertainty, we now use trial three velocities of 5.7, 5.8 and 5.9 km/s to define the crystalline basement, and we then estimate the thickness of the sediment (upper panel Fig. 7a) and consolidated crust between the base of the sediments and the Moho (Fig. 7b). Further, we calculate the corresponding average P-wave speed of the sediment (upper panel Fig. 8a) and consolidated crust (Fig. 8b).

We observe that the combined thickness and average P-wave velocity of the sediment layer and consolidated crust (in Figs. 7 and 8) vary considerably among these three blocks. This variability suggests that the three blocks may have independent origins and deformation histories. All curves along the profile, including the crystalline basement depth (Fig. 7a), consolidated crustal thickness (Fig. 7b), and the corresponding average seismic velocities (Fig. 8a, b) change abruptly at the northern margin fault of the Qinling Mountains between the Qaidam–East Kunlun–West Qinling block and the Central Qilian block, the Maxianshan fault in the Central Qilian block, and the North Qilian fault that lies between the Central and North Qilian blocks. The northern margin fault of the Qinling Mountains between the Qaidam–East Kunlun–West Qinling block and the Central Qilian block can be recognized to be 0.4 km/s higher beneath the Qaidam–East Kunlun–West Qinling block than beneath the Central Qilian block. The Maxianshan fault separates in the Central Qilian block into a southern part, with clear lateral variation in thickness and velocity, and a northern part with a relatively uniform crustal structure. The North Qilian fault on the four curves corresponds to the abrupt transition between the Central and the North Qilian blocks.

The tectonic blocks in the study area have experienced long-term tectonic events, and their crustal structures reflect complicated imprints on Paleozoic collision and Cenozoic deformation from the collision between Indian and Eurasian plates. Before we determine the particular crustal properties, we make comparisons between the global average crustal velocity–depth curve by compiling interpretational results from wide-angle seismic profiles in different parts of the World (Christensen and Mooney, 1995) and tectonic blocks in this study, and provide a similar discussion of depth curves for particular tectonic blocks and compare these with other parts of the continental crust and the Sierra Nevada (Fliedner et al., 2000).

In the Qaidam–Kunlun–West Qinling block and Northern Qilian blocks the P-wave velocity gradient (new curve and existing curves A, C and D, Fig. 9a, b) agrees well with that of the average continental crust (Christensen and Mooney, 1995), but the absolute velocity is lower than the continental average by 0.5 km/s.

In the Central Qilian orogenic belt block, the P-wave velocity gradient (new curve and existing curves A, C and D, Fig. 9c) agrees well with that of the crust beneath the Sierra Nevada (Fliedner et al., 2000). The velocity

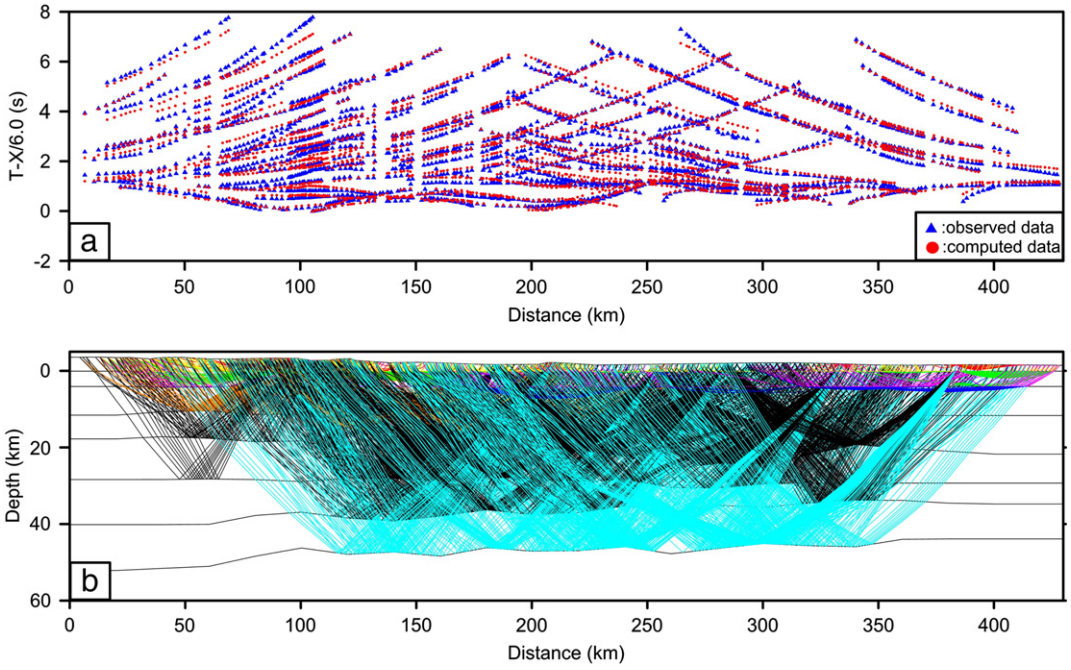

Fig. 4. (a) Comparison between observed (red triangle) and calculated (black circle) travel times for all crustal reflection events obtained from the 11 shot gathers; there is consistently good agreement between the observed and calculated travel times for all recognized seismic events. (b) Summary diagram showing the seismic coverage of the whole crust along the profile.

structure beneath the Central Qilian block seems to be more or less uniform throughout the whole crust, which shows a seismic P-wave velocity distribution deviating not more than 0.2 km/s from a background of 6.0 km/s. This unusual lower crustal velocity gradient points to a more felsic composition of the lower crust than normal for the Central Qilian block, which can be inferred by comparing with the global average (Christensen and Mooney, 1995; Fliedner et al., 2000; Zhang et al., 2011a,b,c,d).

Seismic P-wave velocities are low beneath the Qaidam–Kunlun–West Qinling block and Northern Qilian blocks, and also the Central Qilian orogenic belt block, which may suggest a more felsic continental crust and a more felsic continental arc, respectively. There are also other alternative explanations of these low velocities beneath our profile, such as that the crust is 500 °C above typical continental geotherms, which decreases the seismic velocities (Christensen, 1979). If this is the case, then the crustal Vp/Vs ratios should be much higher than 1.73 because the Vs values will be much lower (Zhang et al., 2009, 2010a,b), which is not consistent with the lower crustal Vp/Vs ratios obtained from areal H–K scanning results (Tian and Zhang, in press) in northeastern Tibet, where a very low Vp/Vs ratio of 1.63 is observed beneath the interior of the Northeastern Tibetan plateau (NETP), in comparison with a higher Vp/Vs ratio of about 1.88 beneath the NETP margins (deformation-resistant areas).

6.3. Constraints on Caledonian orogeny and its activation

6.3.1. Caledonian subduction- or accretion-type orogeny?

In the northern margin of the Tibetan plateau, the Qilian early Paleozoic orogenic belt (or the Qilian–Altyn early Paleozoic orogenic belt, since previous research shows that the Altyn orogenic belt is at the western extent of the Qilian orogenic belt, refer to the section on the geological setting for details) is considered to be an important component of the Tethyan orogenic system. In contrast to the central Asian orogenic belt to the north, which has a long history of accretion (Sengör and Burtman, 1993; Sengör and Okay, 1992; Windley et al., 2007), the Tethyan orogenic system is considered to be the result of the collision of different continental blocks from northern Gondwana (Argand, 1924; Dewey et al., 1988; Sengör, 1987; Yin and Harrison, 2000). However, the Qilian orogenic belt has also been described as an accretionary type (Gehrels et al., 2003a,b; Sengör and Natal'in, 1996; Sengör and Okay, 1992; Xiao et al., 2009).

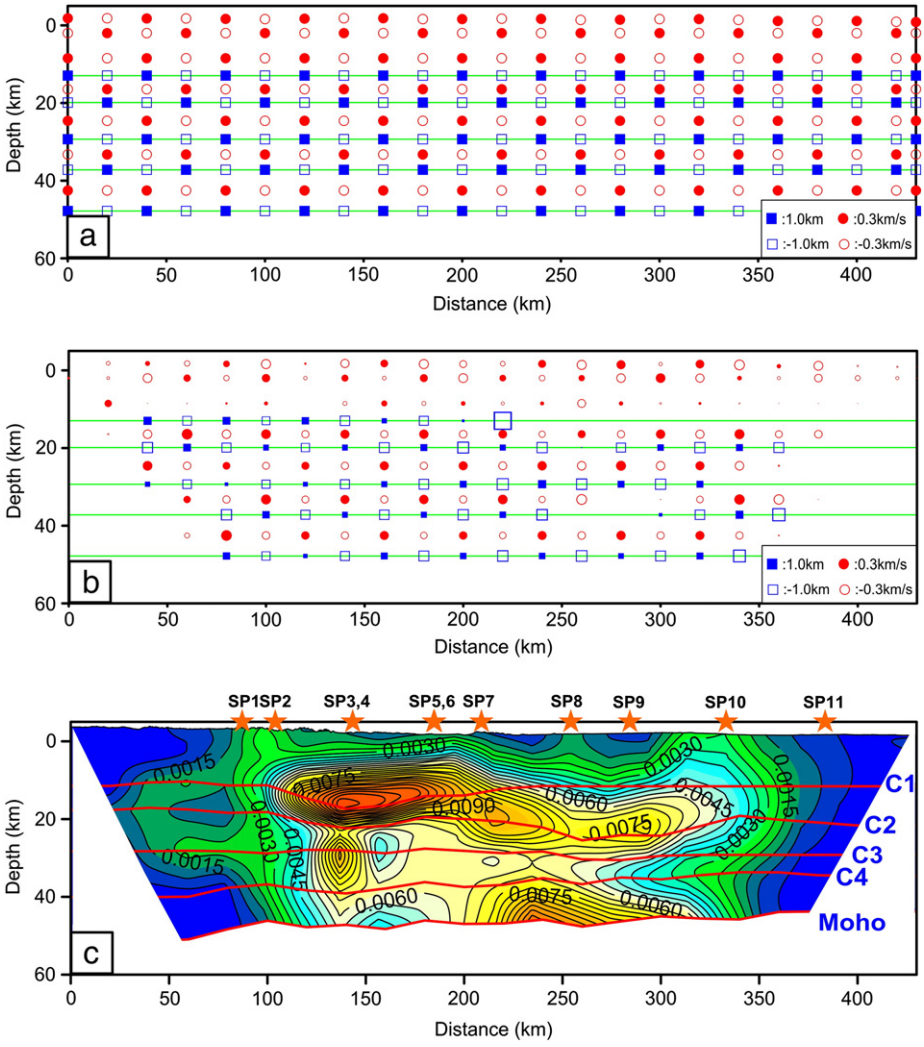

Fig. 5. Assessment of final constructed crustal P-wave velocity model of Fig. 3. To run a Check-board test, (a) We added a velocity perturbation of ±0.3 km/s to each velocity node and a depth perturbation of ±1.0 km to each reflector node in the initial velocity model in order to obtain synthetic travel time data before inversion. Our inversion results (b) show that around the central part of the profile the HVA and LVA are alternately distributed and resemble the checkboard model in (a). This could provide a validation of our final crustal velocity model within the central part area of the profile; (c) Objective function variation in the travel time inversion (Zelt and Smith, 1992) to a P-wave velocity perturbation of 0.3 km/s at each node in the background of our final crustal velocity model. From this, it may be seen that the shallow velocity distribution is more sensitive than the deeper velocity distribution in the travel time inversion of the crustal structure, which implies that the shallow structure and the central portion of crustal structure are more reliable.

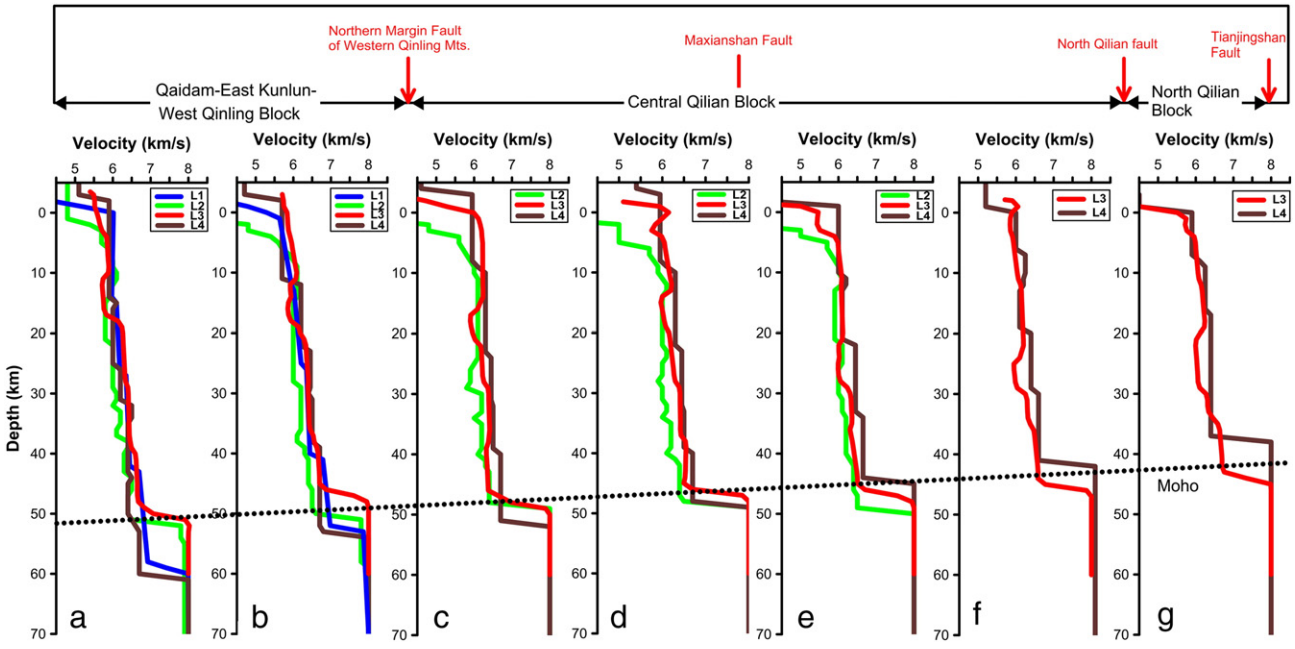

Fig. 6. Comparison between the velocity–depth functions of the Qaidam–East Kunlun–West Qinling block (panels A and B), the Central Qilian (CQ) block (panels C, D, E and F), and the Northern Qilian (NQ) block (panel G) using the profiles passing through the corresponding terranes shown in this figure. From comparison we can observe the variation of crustal structure in both the west–east and north–south directions using Vp–depth curves in and among the panels of the terrane.

The Qilian Caledonian orogenic belt is the product of the convergence and collision orogeny of the Alax, Qilian and Qaidam terranes during the Early Paleozoic (Xu et al., 2001). The discovery of the 600-km-long North Qaidam subduction–collision complex zone (Xu et al., 2001), composed of ophiolite, an ultra high pressure metamorphic (UHPM) belt (containing coesite) (Yang et al., 1999, 2000a,b), and garnet peridotite (Wang and Chen, 1987; Yang et al., 1994) between the Qilian terrane and the Qaidam terrane, and an integrated study of the tectonic regime of the Caledonian plate, provide a scientific basis for understanding the mechanism of formation and exhumation of the North Qaidam UHPM belt. Numerous models have been proposed to explain the Qilian Caledonian orogenic belt, such as the model of the transition from oceanic subduction to continental subduction (Song, 1996; Song et al., 2002, 2006, 2007, 2009; Xu and Cui, 1996; Xu et al., 1994, 1997, 1999; Yang et al., 1998, 2002) and the multi-accretionary model. In the first model, Yang et al. (1998) proposed a paired subduction model; Song et al. (2002, 2009) later proposed a transition model from oceanic to continental subduction. Yin et al. (2007a,b) proposed a diapirism flow model to explain the return of UHPM rocks. There is still some disagreement about the subduction polarity, the collision time, and other aspects. Nevertheless, these models can be summarized in two components: (1) northward deep subduction of the oceanic crust and the continental crust, and formation of the UHPM belt around 500–470 Ma; and (2) Caledonian collision-orogeny of the S. Qilian and exhumation of the UHPM belt around 480–440 Ma. All these arguments are considered in the review by Xiao et al. (2009). Our major problem in evaluating the foregoing models is to verify the existence of oceanic crust beneath the central and the Northern Qilian blocks. From our crustal velocity model, and the crustal properties beneath the central and the Northern Qilian blocks, the crust beneath the central Qilian block shares similar Vp–depth curve characteristics with the Sierra Nevada crust, which has an anomalously lower velocity value in the lower crust?

Our evaluation of the crustal properties of the Central Qilian block from crustal Vp–depth curves (Fig. 9c) demonstrates how the Central Qilian crust is similar to the crust beneath the Sierra Nevada (Fliedner et al., 2000), but has a P-wave velocity about 0.5 km/s lower than the Cenozoic or even the Mesozoic arc. This may suggest that the crust must have looked very different from the present Central Qilian crust if it was a typical continental arc, because the geothermal activity should have been much greater at that time. The 1D crustal column of an average continental arc consists of an upper and middle crust with a thickness of 22 km and a lower crust with a thickness of 16 km and a velocity of 6.8–7.0 km/s (Fliedner et al., 2000; Holbrook et al., 1992), similar to a 7.0–7.5 km/s in the exposed arc section in Pakistan (Miller and Christensen, 1994). The missing lower crust in our crustal velocity model (Fig. 3) should have a mafic composition with a high velocity, and would have been present during arc formation. We speculate that there was southward subduction of the oceanic crust beneath the Central Qilian block (Maxianshan fault), ecologitized with crustal thickening (to >70 km thick with the assumption of similar proportions of the upper/middle/lower crust) during the Caledonian orogeny from oceanic crust subduction. Our inferences may be consistent with a material record of a typical oceanic-type subduction-zone in the early Paleozoic (Wu et al., 1993; Xiao et al., 1978), such as ophiolite suites with zircon SHRIMP U–Pb ages of 495–560 Ma (Shi et al., 2004; Yang et al., 2002), calc-alkaline volcanic and I-type granitic rocks (464 + −8 Ma, Wu et al., 2004), and subduction-zone complexes including HP metamorphic rocks and mélange. Recent studies emphasize the possibility of an oceanic suture zone during the early Paleozoic (440–560 Ma) between the North China craton (NCC) and the Qilian–Qaidam micro-continent, a fragment of the Rodinia supercontinent (Song et al., 2006; Wan et al., 2001).

Our observation that the P-wave velocity ranges from low to 6.1–6.2 km/s beneath the Central Qilian block, with similar Vp–depth curves as the Sierra Nevada crust (Fliedner et al., 2000), cannot exclude the possibility that the Caledonian orogeny beneath the Qilian is accretionary in nature. Fig. 9d shows the comparison of the Vp–depth curve between the Central Qilian block and the accretionary crust (Christensen and Mooney, 1995). The two curves exhibit very similar characteristics from the upper to the lower crust with velocities 0.3–0.5 km/s lower in the lower crust. Another important issue in the possibility of accretion-type orogeny is the concurring appearances of HP/LT metamorphism in the Northern Qilian block (the North Qilian HP metamorphic belt records cold oceanic lithosphere subduction with a low geothermal gradient of 6–7 °C/km) in the early Paleozoic and high temperature

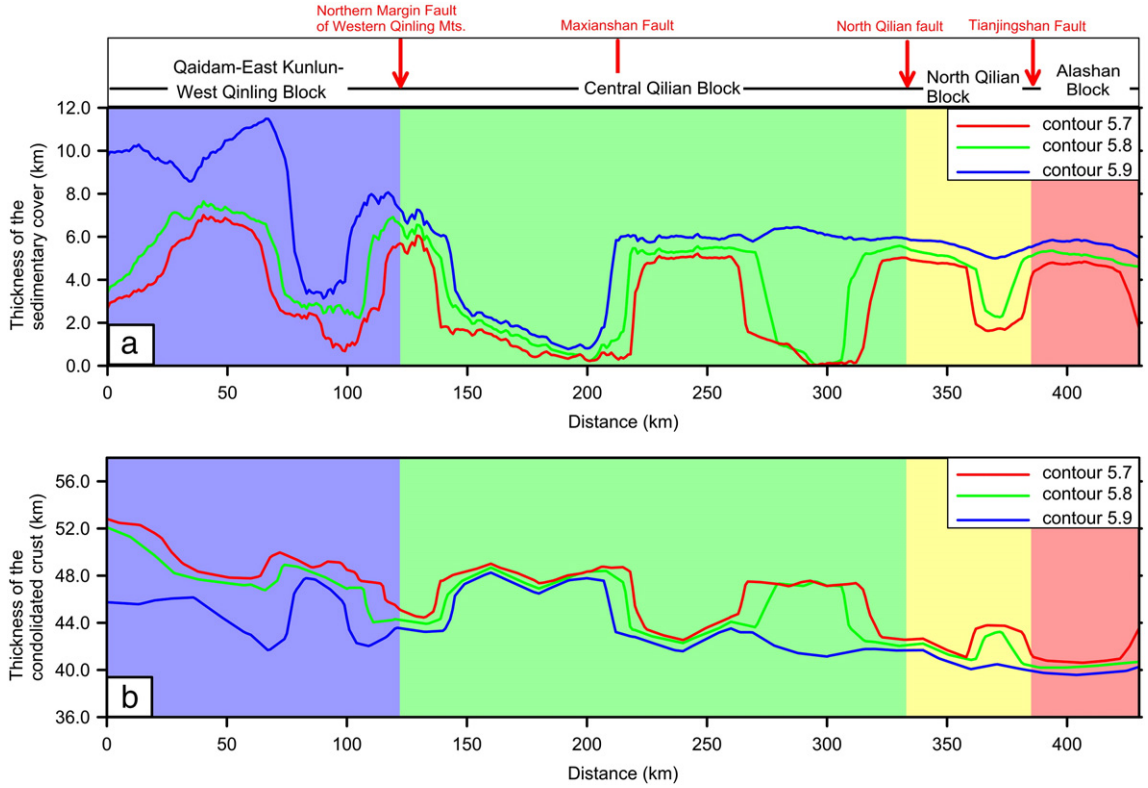

Fig. 7. Laterally varying thicknesses of the sediment layer (a) and variable depth of the consolidated crust (b) along the Jingtai–Hezuo seismic profile.

(HT) metamorphism in the Central Qilian (anomalously lower velocity in the lower crust), which meets the requirement for accretionary orogeny (Xiao et al., 2009; Zhang et al., 2012a,b).

6.3.2. Cenozoic activation (the growth of the plateau) from the collision between the Indian and Eurasian plates

With such a vast amount of data in terms of surface mapping, tectonic, and petrological studies, it is accepted that the HP/LT and UHP metamorphic belts at the northern and southern side of Qilian block are an integral part of the early Paleozoic Qilian orogenic system in northern Tibet (Gehrels et al., 2003a,b; Hsü et al., 1995; Sengör and Natal'in, 1996; Sobel et al., 2001; Yin and Nie, 1993; Yin et al., 2002; Zhang et al., 1984) (Fig. 2). Thanks to the Cenozoic Indo-Asian collision and Mesozoic intracontinental deformation, the original configuration of the Paleozoic Qilian orogen has been significantly modified (Chen et al., 2004; Gehrels et al., 2003a,b; Yin and Harrison, 2000). As a result, understanding the evolution of the early Paleozoic Qilian orogen requires a detailed knowledge of the Cenozoic and Mesozoic deformation history and the effects of these on Paleozoic structures. GPS measurements across northeastern Tibet show that this region is moving NE-NNE at velocities of 19–15 mm/yr relative to the South China block (Gan et al., 2007). However, localities in the foreland, north of the Altyn Tagh fault and Qilian Shan, display much lower and more northerly velocities of 4–10 mm/yr relative to South China (Gan et al., 2007), indicating that the northeastern part of the plateau is moving eastwards relative to the northern foreland. This NE-SW shortening or crustal thickening process in northeastern Tibet, or northward outgrowth of the plateau, was realized from successive accretion of thickening crustal wedges above decollements rooting into south-dipping, lithospheric-mantle subduction zones, initiated along older sutures (Meyer et al., 1998; Tapponnier et al., 2001).

The expansion or growth of the Tibetan plateau is closely related to the strike-slip deformation that dominates the northern part of the Tibetan plateau (Tapponnier et al., 1990, 2001). It has been suggested that left slip at the eastern termination of the Altyn Tagh fault is absorbed by northeast-directed shortening, accommodating growth of the northeastern part of the plateau (Meyer et al., 1998), whereas transpressional deformation is occurring in the Liupan Shan at a southward bend in the east-southeast striking Haiyuan fault. Based on the age of magmatism, deformation, and the seismic structure of the lithosphere at significant tectonic boundaries in the plateau, it has been suggested that deformation took place from south to north, causing stepwise uplift of the Tibetan plateau (Tapponnier et al., 2001). North of the Qaidam–Kunlun–West Qinling block, most of the ESE motion of the Qilian crustal slivers ought to be transferred to the Haiyuan fault, which meets the SE extremities of the Qilian ranges (Meyer et al., 1998). It has been speculated that crustal shortening of 100–200 km above a decollement underlying much of the region requires concurrent Late-Cenozoic shortening and foundering of the lithospheric mantle of that region south of the Kunlun range (Meyer et al., 1998; Tapponnier et al., 2001). From our crustal velocity model (Fig. 3), we observe that there is a 5-km-thick lower velocity layer between the upper and lower crust beneath the northern segment of the profile. This lower velocity layer, deepening from north to south, is probably a seismic signature of the intracrustal decollement layer, even though we could exclude decoupling between the crust and mantle as proposed by Meyer et al. (1998) and Tapponnier et al. (2001). The Tibetan plateau is expanding through the transfer to the northeast of Tibet along the intracrustal decollement. Fig. 3 illustrates that there is an approximately 5-km-thick lower velocity layer (LVL) at the bottom of the upper crust, northwards to the middle of the central Qilian block. We infer that this LVL plays an important role as an intracrustal decollement to accommodate the shortening between the North China craton and the Kunlun terrane and to expand the plateau. It is worth stressing that the concurrent Late-Cenozoic shortening and foundering of the lithospheric mantle of that region south of Kunlun range (Meyer et al., 1998; Tapponnier et al., 2001) cannot be confirmed by the results of our experiments. Recent studies of receiver functions in northeastern Tibet (Zhang et al., 2012b) demonstrate the interesting lateral variation in lithospheric thickness, where this reduces from about 120 to 140 km beneath the QDM–EKL–WQL terrane, 140–

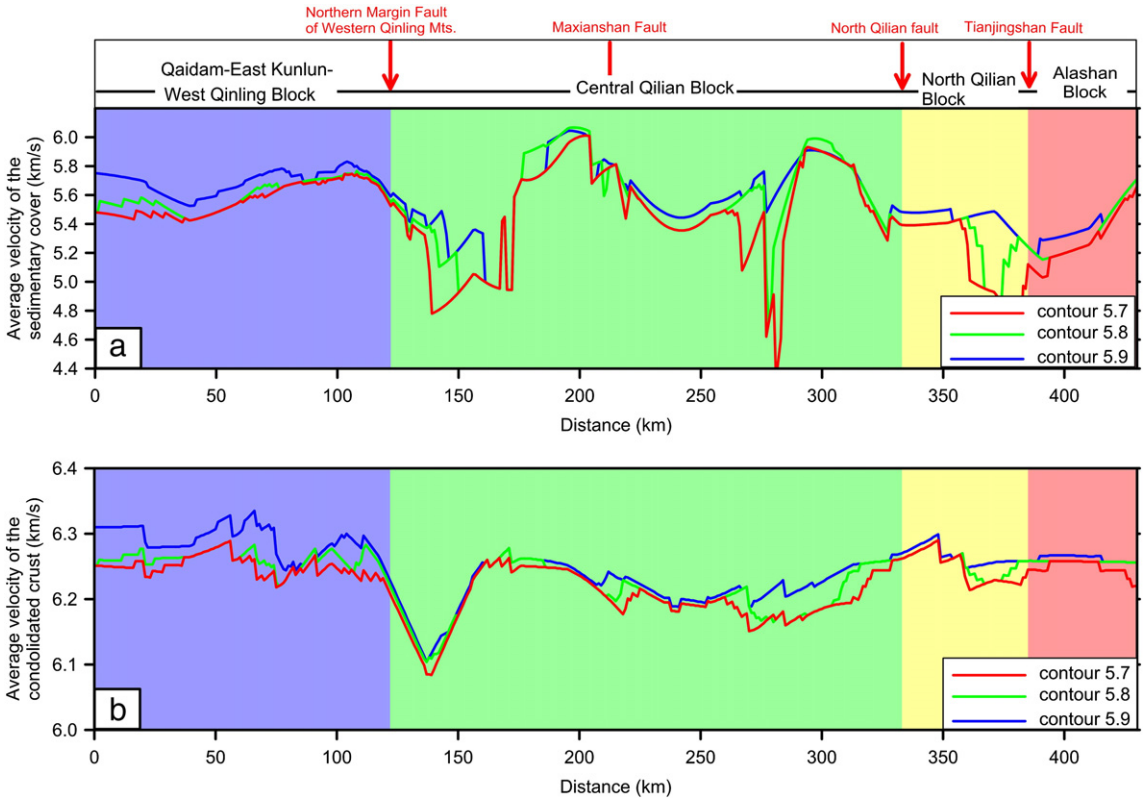

Fig. 8. Average P-wave velocity of the sedimentary layer (a) and the consolidated crust (b) along the Jingtai–Hezuo profile.

150 km beneath the central and the north Qilian block, to about 200 km beneath Alax block (the western North China craton). This asymmetry between the northeastward thinning of crust and lithospheric thickening may provide some indicators for the understanding the possible concurrent Late-Cenozoic shortening and foundering of the lithospheric mantle.

7. Concluding remarks

From the interpretation of a 420-km-long wide-angle seismic profiling across the northeastern Tibetan plateau, we propose the following preliminary conclusions:

(1) Three tectonic blocks lie across the Jingtai–Hezuo profile, namely the Qaidam–Kunlun–West Qinling terrane, the central and the Northern Qilian blocks. These can be distinguished from their seismic properties, such as the average P-wave velocities for the sedimentary layer and consolidated crust. The crust appears to be thinning in a stepwise fashion, in contrast to lithospheric thickening from the Qaidam–Kunlun–West Qinling terrane to the Northern Qilian block.

(2) The Qaidam–Kunlun–West Qinling is characterized by a low vertical velocity gradient and low velocities (compared to the average for the continental crust, though higher than adjacent flysch accumulations), and is inferred to be a continental arc, juxtaposed against the Central Qilian block by the northern margin fault of the West Qinling mountains.

(3) Our crustal velocity model suggests that the crust of the Qaidam–Kunlun–West Qinling terrane is continental, as demonstrated by tectono-stratigraphic characteristics of continent crustal remnants in the central-western sector of the North Qilian Orogeny (Zuo et al., 2002). The crust beneath the Central Qilian block has similar velocity–depth curves to the Sierra Nevada, and suggests that the oceanic crust was ecologized and delaminated, and the continental sediments subducted into the lower crust with the oceanic crust, including partial melting.

(4) The lower velocity layer beneath the central and the Northern Qilian blocks, which shallows from south to north, plays a role as an intracrustal decollement, which suggests the decoupling deformation between the upper and lower crust. The underthrust above the decollement plays a role in the expansion of the plateau, while the lower crustal flow may also contribute to compensate the Late-Cenozoic shortening as supported by the NW predominant direction of fast-splitting shear wave polarization (Zhang et al., 2012a,b).

Acknowledgment

The authors gratefully acknowledge the financial support of the Sinoprobe-02-02, the Chinese Academy of Sciences (KZCX2-YW-132) and the National Nature Sciences Foundation of China (40721003, 40830315 and 41021063). We would also like to thank all the technicians, scientists, and other workers from the Institute of Geology and Geophysics; the Chinese Academy of Sciences; the Geology Samples Centre and the 6th Geophysical Exploration Brigade of the Ministry of Land and Resources (MLR); for their efforts in hole-drilling, source triggering, and in the acquisition of seismic field data. We would particularly like to thank J.E. Vidale and C.A. Zelt for providing the inversion software used in this study. Profs. Bielik and Kind, Drs. Nedunchezhiyan and Jolivet and other reviewers are also appreciated for their constructive comments and suggestions to improve the presentation of the paper.

References

Ammon, C.J., Vidale, J.E., 1993. Tomography without rays. Bulletin of the Seismological Society of America 83 (2), 509–528.
Argand, E., 1924. La tectonique de l'Asie. Proc. 13th Int. Geol.Cong., 7, pp. 171–372.
Beamount, C., Jamieson, R.A., Medvedev, S., 2004. Crustal channel flows: numerical models with applications to the tectonics of the Himalayan–Tibetan orogen. Journal of Geophysical Research 109 (B6), 29.
Burchifel, B., Molnar, P., Zhao, Z., Liang, K., Wang, S., Huang, M., Sutter, J., 1989. Geology of Ulugh Muztagh area, northern Tibet. Earth and Planetary Science Letters 94, 57–70.

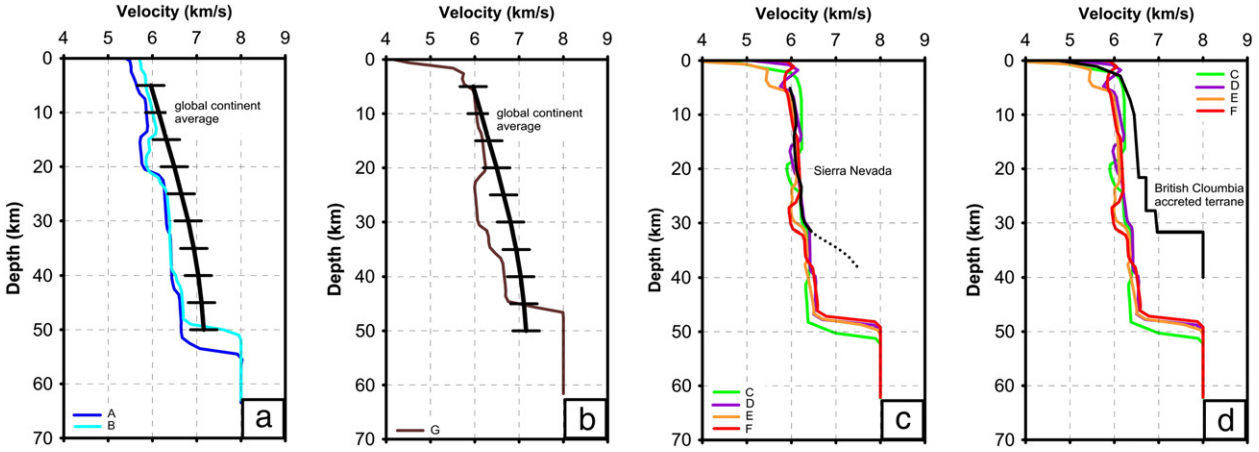

Fig. 9. (a) Comparison between velocity–depth functions for Qaidam–East Kunlun–West Qinling block (transects A and B, Figs. 1 and 6) and a hypothetical average global continent (Christensen and Mooney, 1995); (b) as (a) for the North Qilian (NQ) block (transect G, Figs. 1 and 6); (c) as (a) for the Central Qilian (CQ) block (transects C, D, E and F, Figs. 1 and 6) and the continental arc of the southern Sierra Nevada (Fliedner et al., 2000); (d) as (a) for the Central Qilian (CQ) block (transects C, D, E and F, Figs. 1 and 6) and the accretionary model of British Colombia, poorly constrained by P-wave velocities at the upper most mantle (Christensen and Mooney, 1995). Regarding our wide-angle seismic experiment studied, the velocity–depth curves for the upper mantle are extracted from Pn travel time tomography results (Liang and Song, 2006) and plotted using dashed lines.

Bureau of Geology and Mineral Resources of Ningxia Province, 1990. Regional geology of Ningxia province. Geological Memoirs of Ministry of Geology and Mineral Resources of People's Republic of China.Geological Publishing House, Beijing (in Chinese).

Cerveny, V., Psencik, I., Klimes, L., 1984. Paraxial ray approximations in the computation of seismic wavefields in inhomogeneous media. Geophysical Journal of the Royal Astronomical Society 79 (1), 89–104.

Chen, Z.L., Wang, X.F., Yin, A., Chen, B.L., Chen, X.H., 2004. Cenozoic left-slip motion along the Central Altyn Tagh fault as inferred from the sedimentary record. International Geology Review 46, 839–856.

Christensen, N.I., 1979. Compressional wave velocities in rocks at high temperatures and pressures, critical thermal gradients, and crustal low-velocity zones. Journal of Geophysical Research 84 (B12), 6849–6857.

Christensen, N.I., Mooney, W.D., 1995. Seismic velocity structure and composition of the continental crust: a global view. Journal of Geophysical Research 100, 9761–9788.

Dewey, J.F., Burke, K., 1973. Plume-generated triple junctions: key indicators in applying plate tectonics to old rocks. Journal of Geology 81 (4), 406–433.

Dewey, J.F., Shackelton, R.M., Chang, C., Sun, Y., 1988. The tectonic evolution of the Tibetan plateau. Philosophical Transactions of the Royal Society of London 379–413.

England, P., Houseman, G., 1986. Finite strain calculations of continental deformation. 2. Comparison with the India–Asia collision zone. Journal of Geophysical Research 91 (3), 3664–3676.

England, P., Houseman, G., 1989. Extension during continental convergence, with application to the Tibetan plateau. Journal of Geophysical Research 94, 17561–17579.

Fang, X.M., 1995. The origin and provenance of Malan loess along the eastern margin of Qinghai–Xizang (Tibetan) Plateau and its adjacent area. Science in China. Series B 38 (7), 876–887.

Fang, X.M., Garzione, C., Van der Voo, R., Li, J.J., Fan, M.J., 2003. Flexural subsidence by 29 Ma on the NE edge of the Tibet from the magnetostratigraphy of the Linxia basin, China. Earth and Planetary Science Letters 210, 545–560.

Fang, X.M., Yan, M.D., van der Voo, R., Rea, D.K., Song, C.H., Pares, J.M., Gao, J.P., Nie, J.S., Dai, S., 2005. Late Cenozoic deformation and uplift of the NE Tibetan plateau: evidence from high-resolution magnetostratigraphy of the Guide basin, Qinghai Province, China. Geological Society of America Bulletin 117, 1208–1225.

Feng, Y.M., He, S.P., 1995. Research for geology and geochemistry of several ophiolites in the North Qilian Mountains, China. Geological Review 40, 252–264 (in Chinese with English abstract).

Fliedner, M., Klamperer, S.L., Christensen, N.I., 2000. Three-dimensional seismic model of the Sierra Nevada arc, California, and its implications for crustal and upper mantle composition. Journal of Geophysical Research 105 (B5), 10889–10921.

Gan, W.J., Zhang, P.Z., Niu, Z.J., Shen, Z.K., Wang, M., Wan, Y.G., Zhou, D., Jia, C., 2007. Present-day crustal motion within the Tibetan plateau inferred from GPS measurements. Journal of Geophysical Research 112 (B8), 8416.1–8416.14.

Gansu Bureau of Geology and Mineral Resources, 1989. Regional Geology of Gansu Province. Geologic Publishing House, Beijing, p. 690 (in Chinese with English summary).

Gao, E., 1990. Crustal structure interpreted from the explosive seismic exploration in the Himalayas Yarlung–Zangbo area. In: Li, G., Yuan, X., Hirn, A. (Eds.), Papers on Geophysics, Geology of the Himalayas, vol. 1. Geological Publishing House, Beijing, China, pp. 25–36 (298 pp.).

Garzione, C.N., Ikari, M.J., Basu, A.R., 2005. Source of Oligocene to Pliocene sedimentary rocks in the Linxia basin in northeastern Tibet from Nd isotopes: implications for tectonic forcing of climate. GSA Bulletin 117 (9–10), 1156–1166.

Gehrels, G.E., Yin, A., Wang, X.F., 2003a. Magmatic history of the Altyn Tagh. Journal of Geophysical Research 108 (B9), 2423.

Gehrels, G.E., Yin, A., Wang, X.F., 2003b. Detrital-zircon geochronology of the northeastern Tibetan plateau. Geological Society of America Bulletin 115 (2003), 881–896.

Hirn, A., 1988. Features of the crust–mantle structure of Himalayas–Tibet: a comparison with seismic traverses of Alpine, Pyrenean and Variscan Orogenic Belts. Philosophical Transactions of the Royal Society of London. Series A 326, 17–32.

Hirn, A., Damotte, B., Torreilles, G., 1987. Crustal reflection seismics: the contributions of oblique, low frequency and shear wave illuminations. Geophysical Journal of the Royal Astronomical Society 89, 287–296.

Holbrook, W.S., Mooney, W.D., Christensen, N.I., 1992. The seismic velocity structure of the deep continental crust. In: Fountain, D.M., Arculus, R., Kay, R.W. (Eds.), Continental Lower Crust. Elsevier Sci., New York, pp. 1–43.

Hole, J.A., Zelt, B.C., 1996. Inversion of three-dimensional wide-angle seismic data from the southwestern Canadian Cordillera. Journal of Geophysical Research 101 (B4), 8503–8529.

Hsü, Kenneth J., Pan, G.T., Sengör, A.M.C., 1995. Tectonic evolution of the Tibetan plateau: a working hypothesis based on the archipelago model of orogenesis. International Geology Review 37, 473–508.

Huang, J.Q., 1977. The basic outline of China tectonics. Acta Geologica Sinica 52, 117–135.

Jia, S., Zhang, X.K., Zhao, J., 2009. Deep seismic sounding data reveals the crustal structures beneath Zoige basin and its surrounding folded orogenic belts. Science in China Series D: Earth Sciences 39 (9), 1200–1208 (in Chinese).

Jiang, M., Galvé, A., Hirn, A., de Voogd, B., Laigle, M., Su, H.P., Diaz, J., Lépine, J.C., Wang, Y.X., 2006. Crustal thickening and variations in architecture form the Qaidam basin to the Qang Tang (North-Central Tibetan plateau) from wide-angle reflection seismology. Tectonophysics 412, 121–140.

Klemperer, S.L., 2006. Crustal flow in Tibet: a review of geophysical evidence for the physical state of Tibetan lithosphere. In: Searle, M.P., Law, R.D. (Eds.), Channel flow, ductile extrusion and exhumation of lower mid-crust in continental collision zones: Geol. Soc. Spec. Publ., 268, pp. 39–70.

Li, S.L., Mooney, W.D., 1998. Crustal structure of China from deep seismic sounding profiles. Tectonics 288, 105–113.

Li, Q.S., Peng, S.P., Gao, R., Fan, J.Y., 2003. Seismic evident of the basement uplift in the Bayan Har tectonic belt, Qinghai, and its tectonic significance. Geological Bulletin of China 22 (10), 782–788.

Liang, C., Song, X., 2006. A low velocity belt beneath northern and eastern Tibetan plateau from Pn tomography. Geophysical Research Letters 33, L22306.

Liou, J.G., Graham, S.A., 1989. Proterozoic blueschist belt in western China: best documented Precambrian blueschists in the world. Geology 17, 1127–1131.

Liu, M.J., Mooney, W.D., Li, S.L., Okaya, N., Detweiler, S., 2006. Crustal structure of the northeastern margin of the Tibetan plateau from the Songpan–Ganzi Terrane to the Ordos Basin. Tectonophysics 420 (1–2), 253–266.

Luetgert, J.H., 1988. User's manual for RAY84/R83PLT interactive two-dimensional raytracing synthetic seismogram package. Geological Survey 88–238.

Makovsky, Y., Klemperer, S.L., Ratschbach, L., Alsdotf, D., 1999. Midcrustal reflector on INDEPTH wide-angle profiles: an ophiolitics lab beneath the India–Asia suture in southern Tibet. Tectonics 18, 793–808.

Mattauer, M., 1986. Intracontinental subduction, crust–mantle decollement and crustal-stacking wedge in the Himalayas and other collision belts. Geological Society, London, Special Publications 37–50.

Meng, Q.R., Zhang, G.W., 2000. Geologic framework and tectonic evolution of the Qinling orogen, central China. Tectonophysics 323 (3–4), 183–196.

Metivier, F., Gaudemer, Y., Tapponnier, P., Meyer, B., 1998. Northeastward growth of the Tibet Plateau deduced from balanced reconstruction of two depositional areas: the Qaidam and Hexi Corridor basins, China. Tectonics 17, 823–842.

Meyer, B., Tapponnier, P., Bourjot, L., Metivier, F., Gaudemer, Y., Peltzer, G., Guo, S., Chen, Z., 1998. Crustal thickening in Gansu–Qinghai, lithospheric mantle subduction, and oblique, strike-slip controlled growth of the Tibet Plateau. Geophysical Journal International 135, 1–47.

Miller, D.J., Christensen, N.I., 1994. Seismic signature and geochemistry of an island arc: a multidisciplinary study of the Kohistan accreted terrane, northern Pakistan. Journal of Geophysical Research 99, 6865–6880.
Min, Z., Wu, F., 1987. Nature of the upper crust beneath central Tibet. Earth and Planetary Science Letters 84, 204–210.
Molnar, P., 1993. Mantle dynamics, uplift of the Tibetan plateau, and the Indian Monsoon. Reviews of Geophysics 31 (4), 357–396.
Molnar, P., Lyon-Caen, H., 1988. Some simple physical aspects of the support, structure, and evolution of mountain belts. Geological Society of America Special Paper 179–207.
Molnar, P., Tapponnier, P., 1978. Active tectonics of Tibet. Journal of Geophysical Research 83 (11), 5361–5375.
Mooney, W.D., Braile, L.W., 1989. The Seismic Structure of the Continental Crust and Upper Mantle of North America, the Geology of North America. Geological Society of America, pp. 39–52.
Nelson, K.D., Zhao, W., Brown, L.D., Brown, L.D., Kuo, L., Che, J., Liu, X., Klemperer, S.L., Makovsky, Y., Meissner, R., Mechie, J., Kind, R., Wenzel, F., Ni, J., Nabelek, J., Leshou, C., Tan, H., Wei, W., Jones, A.G., Booker, J., Unsworth, M., Kidd, W.S.F., Hauck, M., Alsdorf, D., Ross, A., Cogan, M., Wu, C., Sandvol, E., Edwards, M., 1996. Partially molten middle crust beneath southern Tibet: synthesis of project INDEPTH results. Science 274, 1684–1688.
Owens, T.J., Zandt, G., 1997. Implications of crustal property variations for models of Tibetan plateau evolution. Nature 387 (627), 37–43.
Royden, L.H., Burchfiel, B.C., Van der Hilst, R.D., 2008. The geological evolution of the Tibetan plateau. Science 321 (5892), 1054–1058.
Sengör, A.M.C., 1987. Tectonics of the Tethysides: orogenic collage development in a collisional setting. Annual Review of Earth and Planetary Sciences 15, 213–244.
Sengör, A.M.C., Burtman, V.S., 1993. Evolution of the Altaid tectonic collage and Palaeozoic crustal growth in Eurasia. Nature 364 (6435), 299–307.
Sengör, A.M.C., Natal'in, B.A., 1996. Turkic-type orogeny and its in the making of the continental crust. Annual Review of Earth and Planetary Sciences 263–337.
Sengör, A.M.C., Okay, A.I., 1992. Evidence for intracontinental thrust-related exhumation of the ultra-high-pressure rocks in China. Geology 411–14.
Shi, R.D., Yang, J.S., Wu, C.L., Tsuyushi, L., Takakumi, H., 2004. Island arc volcanic rocks in the north Qaidam UHP metamorphic belt. Acta Geologica Sinica 78, 52–64.
Sobel, E.R., Arnaud, N., Jolivet, M., Ritts, B.D., Brunel, M., 2001. Jurassic to Cenozoic exhumation history of the Altyn Tagh range, northwest China, constrained by $^{40}Ar/^{39}Ar$ and apatite fission track thermochronology. Geological Society of America Memoir 194, 247–266.
Song, S.G., 1996. Metamorphic evolution of the coesite-bearing ultrahigh-pressure terrane in the North Qaidam, Northern Tibet, NW China. Journal of Metamorphic Geology 21 (6), 631–644.
Song, S.G., Yang, J.S., Xu, Z.Q., Zhang, J.X., Wu, C.L., Shi, R.D., Li, H.B., Brunel, M., 2002. Early Palaeozoic North Qaidam UHP metamorphic belt on the northeastern Tibetan plateau and a paired subduction model. Terra Nova 14 (5), 397–404.
Song, S.G., Zhang, L.F., Niu, Y.L., Su, L., Song, B., Liu, D., 2006. Evolution from oceanic subduction to continental collision: a case from the Northern Tibetan plateau based on geochemical and geochronological data. Journal of Petrology 47 (93), 435–455.
Song, S.G., Su, L., Niu, Y.L., Zhang, L.F., Zhang, G.B., 2007. Petrological and geochemical constraints on the origin of garnet peridotite in the North Qaidam ultrahigh-pressure metamorphic belt, northwestern China. Lithos 96 (1–2), 243–265.
Song, S.G., Yang, J.S., Zhang, L.F., Wei, C.J., Su, X.L., 2009. Metamorphic evolution of low-T eclogite from the North Qilian orogen, NW China: evidence from petrology and calculated phase equilibria in the system NCKFMASHO. Journal of Metamorphic Geology 27 (1), 55–70.
Tapponnier, P., Meyer, B., Avouac, J.P., Peltzer, G., Gaudemer, Y., Guo, S., Xiang, H., Yin, K., Chen, Z., Cai, S., Dai, H., 1990. Active thrusting and folding in the Qilian Shan and decoupling between upper crust and mantle in northeastern Tibet. Earth and Planetary Science Letters 97, 382–403.
Tapponnier, P., Xu, Z.Q., Roger, F., Meyer, B., Arnaud, N., Wittlinger, G., Yang, J.S., 2001. Oblique stepwise rise and growth of the Tibet plateau. Science 294 (5547), 1671–1677.
Teng, J.W., 1987. Explosion study of the structure and seismic velocity distribution of the crust and upper mantle under the Xizang (Tibet) Plateau. Geophysical Journal of the Royal Astronomical Society 89, 405–414.
Teng, J.W., Zhang, Z.J., Zhang, X.K., Wang, C.Y., Gao, R., Yang, B.J., Qiao, Y.H., Deng, Y.F., in press. Moho discontinuity beneath the continent of Chinese mainland from deep seismic sounding profiling. Tectonophysics. http://dx.doi.org/10.1016/j.tecto.2012.11.024.
Tian, X., Zhang, Z., in press. Bulk crustal properties in NE Tibet and their implications for deformation model. Gondwana Research. http://dx.doi.org/10.1016/j.gr.2012.12.024
Vidale, J.E., 1988. Finite-difference calculation of traveltimes in three dimensions. Geophysics 55 (5), 521–526.
Wan, Y.S., Xu, Z.Q., Yang, J.S., Zhang, J.X., 2001. Ages and compositions of the Precambrian high-grade basement of the Qilian terrane and its adjacent areas. Acta Geologica Sinica — English Edition 75, 375–384.
Wang, Y.X., Chen, J., 1987. Metamorphic Zones and Metamorphism in Qinghai Province and Its Adjacent Areas. Geological Publishing House, Beijing, pp. 213–220 (in Chinese with English abstract).
Wang, Y.X., Mooney, W.D., Han, G.H., Yuan, X.C., Jiang, M., 2005. Crustal P-wave velocity structure from Altyn Tagh to Longmen mountains along the Taiwan–Altay geoscience transect. Chinese Journal of Geophysics 48 (1), 98–106 (in Chinese).
Windley, B.F., Alexeiev, D., Xiao, W.J., Kroner, A., Badarch, G., 2007. Tectonic models for accretion of the Central Asian Orogenic Belt. Journal of Geophysical Research 164 (1), 31–47.
Wu, H.Q., Feng, Y.M., Song, S.G., 1993. Metamorphism and deformation of blueschist belts and their tectonic implications, North Qilian Mountains, China. Journal of Metamorphic Geology 11, 523–536.
Wu, C.L., Yang, J.S., Yang, H.Y., Wooden, J.L., Shi, R.D., Chen, S.Y., Zheng, Q.G., 2004. Dating of two types of granite from north Qilian, China. Acta Petrologica Sinica 425–432 (in Chinese with English abstract).
Xiao, X., Chen, G., Zhu, Z., 1978. The Qilianshan ophiolite and its geological significance. Acta Geologica Sinica 52, 281–295 (in Chinese with English abstract).
Xiao, W.J., Windley, B.F., Yong, Y., 2009. Early Paleozoic to Devonian multiple-accretionary model for the Qilian Shan, NW China. Journal of Asian Earth Sciences 35, 323–333.
Xiong, S.B., Liu, H.B., 1997. Crustal structure in the western Tibetan plateau. Chinese Science Bulletin 42 (12), 1309–1311.
Xu, Z.Q., Cui, J.W., 1996. Deformation Tectonic Dynamics of Continental Mountain Chains. China Metallurgical Industry Press, Beijing, p. 246 (in Chinese with English abstract).
Xu, Z.Q., Xu, H.F., Zhang, J.X., 1994. Caledonian subducted complex accretionary massif and its dynamics in South Zulang Mountains form North Qilian Mountains. Acta Geologica Sinica 68 (1), 1–15.
Xu, Z.Q., Zhang, J.X., Xu, H.F., Wang, Z.X., Li, H.B., Yang, T.N., Qiu, X.P., Zeng, L.S., Shen, K., Chen, W., 1997. Ductile Shear Zone and Its Dynamics of Major Continental Mountain Chains in China. China Geological Press, Beijing, p. 294 (in Chinese with English abstract).
Xu, Z.Q., Yang, J.S., Zhang, J.X., 1999. The Comparison of tectonic units along the sides of Altin faults and the shearing mechanism of lithosphere. Acta Geologica Sinica 73 (3), 193–205 (in Chinese with English abstract).
Xu, Z.Q., Yang, J.S., Zhang, J.X., 2001. Tectonic evolution and lithospheric shearing in the Altun Mts. and Qilian Mts. Research Report, Institute of Geology, Chinese Academy of Geological Sciences (in Chinese, unpublished).
Yang, J.J., Zhu, H., Deng, J.F., Zhou, T.Z., Lai, S.C., 1994. Discovery of garnet–peridotite at the northern margin of the Qaidam basin and its significance. Acta Petrologica et Mineralogica 13, 97–105.
Yang, J.S., Xu, Z., Li, H., Wu, C., Cui, J., Zhang, J.X., Chen, W., 1998. Discovery of eclogite at northern margin of Qaidam basin, NW China. Chinese Science Bulletin 43, 1755–1760.
Yang, J.S., Xu, Z.Q., Zhang, J., Jiang, M., Li, H., Cui, J., 1999. A comparison between the tectonic units on the two sides of the Altun sinistral strike-slip fault and the mechanism of lithospheric shearing. Acta Geologica Sinica 73 (3), 193–205 (in Chinese with English abstract).
Yang, J.S., Xu, Z., Li, H.B., Wu, C.L., Zhang, J.X., Shi, R.D., 2000a. An Early Paleozoic convergent border at the southern margin of the Qilian terrain, NW China: evidence from the ecogite, garnet peridotite and ophiolite. Journal of the Geological Society of China (Taiwan) 43, 142–164.
Yang, J.S., Xu, Z., Song, S., Wu, C., Shi, R., Zhang, J., Wan, Y., Li, H., Jin, X., Jalivet, M., 2000b. Discovery of ecogite in Dulan, Qinghai Province and its significance for the HP–UHP metamorphic belt along the central orogenic belt of China. Acta Geologica Sinica 74, 156–168 (in Chinese with English abstract).
Yang, W.R., Deng, Q.L., Wu, X.L., 2002. Major characteristics of the Lajishan orogenic belt of the south Qilian Mountains and its geotectonic attribute. Acta Geologica Sinica 76 (1), 110–117.
Yin, A., 2010. Cenozoic tectonic evolution of Asia: a preliminary synthesis. Tectonophysics 488, 293–325.
Yin, A., Nie, S., 1993. An indentation model for North and South China collision and the development of the Tanlu and Honam fault systems, eastern Asia. Tectonics 12, 801–813.
Yin, A., Harrison, T.M., 2000. Geologic evolution of the Himalayan–Tibetan orogen. Annual Review of Earth and Planetary Sciences 28 (1), 211–280.
Yin, A., Rumelhart, P.E., Butler, R., Cowgill, E., Harrison, T.M., Foster, D.A., Ingersoll, R.V., Zhang, Q., Zhou, X.Q., Wang, X.F., Hanson, A., Raza, A., 2002. Tectonic history of the Altyn Tagh fault system in northern Tibet from Cenozoic sedimentation. Geological Society of America Bulletin 114, 1257–1295.
Yin, A., Dang, Y.Q., Zhang, M., McRivette, M.W., Burgess, W.P., Chen, X.H., 2007a. Cenozoic tectonic evolution of Qaidam basin and its surrounding regions (part 2): wedge tectonics in southern Qaidam basin and the Eastern Kunlun Range. Geological Society of America Special Papers 433, 369–390.
Yin, A., Manning, C.E., Lovera, O., Menold, C., Chen, X., Gehrels, G.E., 2007b. Early Paleozoic tectonic and thermomechanical evolution of Ultrahigh-pressure (UHP) metamorphic rocks in the Northern Tibetan plateau of NW China. International Geology Review 49, 681–716.
Zelt, C.A., Smith, R.B., 1992. Seismic travel inversion for 2-D crustal velocity structure. Geophysical Journal International 108, 16–34.
Zhang, Z.J., Klemperer, S.L., 2005. West–east variation in crustal thickness in northern Lhasa block, central Tibet, from deep seismic sounding data. Journal of Geophysical Research 110 (B09), 403.1–403.14.
Zhang, Z.J., Klemperer, S.L., 2010. Crustal structure of the Tethya Himalaya, southern Tibet: new constrains from old wide-angle seismic data. Geophysical Journal International 181 (3), 1247–1260.
Zhang, Z.M., Liou, J.G., Coleman, R.G., 1984. An outline of the plate tectonics of China. Geological Society of America Bulletin 95, 295–312.
Zhang, J.X., Meng, F.C., Yang, J.S., 2003. Eclogitic metapelites in the western segment of the north Qaidam basin and their geological implications. Regional Geology of China 22, 655–657.
Zhang, X.K., Jia, S., Zhao, J., 2008. Crustal structures beneath West Qinling–East Kunlun orogen and its adjacent area—Results of wide-angle seismic reflection and refraction experiment. Chinese Journal of Geophysics 51 (2), 439–450 (in Chinese).
Zhang, Z.J., Wang, Y.H., Chen, Y., Tian, X., Houseman, G., Wang, E., Teng, J., 2009. Crustal structure across Longmenshan fault belt from passive source seismic profiling. Geophysical Research Letters 36 (17), 310.1–310.4.
Zhang, J.X., Meng, F.C., Yu, S.Y., 2010a. Two contrasting HP/LT and UHP metamorphic belts: constraints on Early Paleozoic orogeny in Qilian–Altun orogen. Acta Petrologica Sinica 26 (7), 1967–1992.

Zhang, Z.J., Yuan, X., Chen, Y., Tian, X., Kind, R., Li, X., Teng, J., 2010b. Seismic signature of the collision between the east Tibetan escape flow and the Sichuan Basin. Earth and Planetary Science Letters 292, 254–264.
Zhang, Z.J., Yang, L.Q., Teng, J.W., Badal, J., 2011a. An overview of the earth crust under China. Earth-Science Reviews 104 (1–3), 143–166.
Zhang, Z.J., Deng, Y.F., Teng, J.W., Wang, C.Y., Gao, R., Chen, Y., Fan, W.M., 2011b. An overview of the crustal structure of the Tibetan plateau after 35 years of deep seismic soundings. Journal of Asian Earth Sciences 40 (4), 977–989.
Zhang, Z.J., Klemperer, S.L., Bai, Z.M., Chen, Y., Teng, J.W., 2011c. Crustal structure of the Paleozoic Kunlun orogeny from an active-source seismic profile between Moba and Guide in East Tibet, China. Gondwana Research 19 (4), 994–1007.
Zhang, Z.J., Chen, Q.F., Bai, Z.M., Chen, Y., Badal, J., 2011d. Crustal structure and extensional deformation of the thinned lithosphere in North China. Tectonophysics 508, 62–72.
Zhang, H.S., Teng, J.W., Tian, X.B., Zhang, Z.J., Gao, R., Liu, J.Q., 2012a. Lithospheric thickness and upper mantle deformation beneath the NE Tibetan plateau inferred from S receiver functions and SKS splitting measurements. Geophysical Journal International 191 (3), 1285–1294.
Zhang, Z.J., Deng, Y.F., Chen, L., Wu, J., Teng, J.W., Panza, G., 2012b. Seismic structure and rheology of the crust under mainland China. Gondwana Research. http://dx.doi.org/10.1016/j.gr.2012.07.010.
Zhao, W.L., Morgan, W.J., 1985. Uplift of Tibetan plateau. Tectonics 4 (4), 359–369.
Zhao, W., Nelson, K.D., 1993. Deep seismic reflection evidence for continental underthrusting beneath southern Tibet. Nature 366, 557–559.
Zhao, W., Brown, L.D., Guo, J., Haines, S., Mechie, J., Klemperer, S.L., Ma, Y.S., Meissner, R., Nelson, K.D., Ni, J.F., Pananont, P., Rapine, R., Ross, A., Saul, J., 2001. Crustal structure of central Tibet as derived from project INDEPTH wide-angle seismic data. Geophysical Journal International 145, 486–498.
Zuo, G.C., Liu, Y.K., Zhang, C., 2002. Tectono-stratigraphic characteristics of continent crustal remnants in central-western sector of the North Qilian Orogen. Geoscience 37 (3), 302–310 (in Chinese with English abstract).